Monotonic and Cyclic Simple Shear Response of Well-Graded Sandy Gravel Soils from Wellington, New Zealand

Jongchan Kim, Aff.M.ASCE[1]; Adda Athanasopoulos-Zekkos, M.ASCE[2]; and Misko Cubrinovski[3]

Abstract: In the 2016 Kaikoura earthquake, liquefaction of gravelly soils from reclaimed fills occurred in CentrePort, Wellington, New Zealand. This study presents constant volume monotonic and cyclic simple shear tests on well-graded gravel with sand collected from CentrePort. A large-scale cyclic simple shear device is utilized to evaluate the monotonic, cyclic, and postcyclic responses of the sandy gravel soils. Specimens prepared at various relative densities were subjected to a vertical effective stress of 100 kPa and then monotonically and cyclically sheared. After the cyclic loading, the postcyclic response was evaluated, including volumetric compression or monotonic shear with or without dissipation of excess pore water pressure. Shear wave velocity was measured before and after the cyclic loading. The results show that the well-graded sandy gravel has a high potential for liquefaction, with higher relative density specimens having higher liquefaction resistance. Postcyclic volumetric strain is primarily correlated with density and maximum shear strain during cyclic loading. Postcyclic reconsolidation causes densification of the liquefied specimens, resulting in higher monotonic shear resistance, while postcyclic monotonic shear without dissipation of excess pore water pressure reveals that substantial shear strain is required to develop the shear resistance. Shear wave velocity was significantly reduced after liquefaction, but recovered to slightly higher than its precyclic shear values after reconsolidation. Compared to other gravelly and sandy soils, the well-graded sandy gravel showed a similar or slightly higher liquefaction resistance than gap-graded and uniform gravels. Moreover, the well-graded sandy gravel had a relatively lower ultimate postcyclic volumetric strain due to a small variation between its maximum and minimum void ratios. The results advance our understanding of the liquefaction resistance and subsequent postcyclic responses of the well-graded sandy gravel soils. **DOI: 10.1061/JGGEFK.GTENG-10619.**

Author keywords: Cyclic simple shear; Gravelly soils; Liquefaction; Postcyclic response; Shear wave velocity.

Introduction

Soil liquefaction is a phenomenon in which soils behave like liquid due to a reduction in the effective stress and shear resistance (Marcuson 1978; Seed and Lee 1966), resulting in lateral ground displacements, catastrophic damage to structures, and endangerment of human life. This is caused by the generation of excess pore water pressure during dynamic loadings, such as that caused by an earthquake. Many researchers have investigated the liquefaction of sands and mixtures of sands and fine soils (Bray and Sancio 2006; Cappellaro et al. 2021; Monkul et al. 2015; Peacock and Seed 1968, Porcino et al. 2008; Sivathayalan 2000; Vaid and Sivathayalan 1996; Vaid and Finn 1979). In the study of liquefaction, gravelly soils have received less attention than sandy deposits; gravelly soils have been considered less liquefiable because of their higher stiffness and peak shear strength, lower potential for generation of excess pore water pressure, and ability to dissipate the excess pore water pressure faster than sandy soils due to their higher hydraulic conductivity. However, several case histories have reported that earthquakes can cause liquefaction of reclaimed gravelly soils (Athanasopoulos et al. 2020; Cubrinovski et al. 2017a; Hatanaka et al. 1997; Nikolaou et al. 2014, 2015). In the 2016 Kaikoura earthquake, severe liquefaction was observed in gravelly fills at CentrePort, Wellington, New Zealand (Cubrinovski et al. 2017b; Dhakal et al. 2020) that resulted in lateral spreading and displacements of up to 1.0 m. CentrePort is one of the important commercial ports in New Zealand, and the earthquake impacted passenger and cargo transportation for several months, resulting in NZD 28 million in costs for the temporary recovery and stabilization process (Cubrinovski et al. 2020). The port was constructed by two major reclamation projects in 1901–1932 and 1965–1976, and recent cone penetration test (CPT) investigations revealed that the subsurface deposits consist of gravels, sands, and silts with low density, due to the uncompacted manner by which the fills were placed during construction (Dhakal et al. 2020). Following the M_w 7.8 Kaikoura earthquake in 2016, significant liquefaction and gravelly ejecta were observed. The grain size distribution of the gravelly ejecta is identical to that of gravel reclamation fill, indicating that the earthquake caused liquefaction of the gravelly deposits (Cubrinovski et al. 2018). Evaluating the liquefaction potential of gravelly soils and the consequences is important because these materials are encountered in critical infrastructures, such as ports, dams, and levees.

[1]Postdoctoral Researcher, Dept. of Civil and Environmental Engineering, Univ. of California at Berkeley, Berkeley, CA 94720. Email: jkim3139@berkeley.edu

[2]Associate Professor, Dept. of Civil and Environmental Engineering, Univ. of California at Berkeley, Berkeley, CA 94720 (corresponding author). ORCID: https://orcid.org/0000-0002-3785-9009. Email: adda.zekkos@berkeley.edu

[3]Professor, Dept. of Civil and Natural Resources Engineering, Univ. of Canterbury, Christchurch 8041, New Zealand. Email: misko.cubrinovski@canterbury.ac.nz

Note. This manuscript was submitted on December 9, 2021; approved on February 8, 2023; published online on April 26, 2023. Discussion period open until September 26, 2023; separate discussions must be submitted for individual papers. This paper is part of the ***Journal of Geotechnical and Geoenvironmental Engineering***, © ASCE, ISSN 1090-0241.

Considerable effort has focused on field investigations of liquefied gravelly deposits (Andrus and Stokoe 2000; Bolton Seed et al. 1985; Cao et al. 2011, 2013; Cubrinovski et al. 2018; Harder 1997; Kokusho et al. 1995; Lin et al. 2004; Robertson and Wride 1998; Rollins et al. 2022), which is particularly insightful because they provide an opportunity to characterize the material in situ. However, laboratory testing is needed to quantify the influence of several factors affecting liquefaction behavior, including relative density, cyclic loading amplitude, grain size distribution, and confining stress. Many researchers have studied the cyclic shear response of gravelly soils under drained or undrained conditions (Chang et al. 2014; Flora et al. 2012; Hara et al. 2004; Hubler et al. 2017, 2018; Kokusho et al. 2004; Lin et al. 2004; Lin and Chang 2002; Wang and Wang 2017; Wang et al. 2020; Xenaki and Athanasopoulos 2008). Gravelly soils in nature are commonly well-graded with a larger coefficient of uniformity than sands because gravelly soils are mostly mixtures of gravel, sand, and finer particles (Kokusho et al. 2004). Most importantly, the cyclic simple shear test is a particularly well-suited laboratory method to assess liquefaction susceptibility because the simple shear loading causes a rotation of the principal stresses during shear, which simulates the in situ ground response during an earthquake (Seed and Lee 1966; Sivathayalan and Ha 2011), and constant volume simple shear testing allows achieving undrained conditions with no membrane compliance. Therefore, a more detailed understanding of the monotonic and cyclic simple shear response of well-graded gravelly soils and subsequent postcyclic response is particularly valuable.

This paper presents constant volume monotonic and cyclic tests using a large-scale cyclic simple shear device to accommodate the gravel-sized particle [retained by a No. 4 sieve in the Unified Soil Classification System (USCS)]. The device, described in Zekkos et al. (2018), enables the use of reconstituted gravelly specimens with a diameter of 307 mm and a height of about 115 mm. This study aims to experimentally investigate the monotonic and cyclic simple shear response under constant volume conditions of well-graded gravel with sand (per USCS) collected from Wellington, New Zealand. The postcyclic response (i.e., postcyclic volumetric strain by reconsolidation and postcyclic monotonic shear response with and without reconsolidation) were evaluated. Moreover, shear wave velocity was measured before and after the cyclic loading using accelerometers mounted on top and bottom of the specimen (Zekkos et al. 2018). The results were compared to other uniform gravelly and sandy soils from previous studies.

Experimental Study

Test Materials

Gravelly soils were obtained from CentrePort, Wellington, New Zealand, where severe liquefaction and liquefaction-induced settlements were experienced following the M_w 7.8 Kaikoura earthquake in 2016. The samples were collected from borehole TP2 [Fig. 1(a)], at a reclaimed deposit depth of 3.92–10.2 m, and shipped to the University of California at Berkeley for laboratory testing. Details of the site and boreholes were documented in Cbrinovski et al. (2017a, 2018) and Dhakal et al. (2020).

The grain size distribution of the tested material (from borehole TP2, 6.96–7.96 m in depth) is shown in Fig. 1(b), along with other soils from previous studies. The collected soils were oven-dried and sieved with dry- and wet-sieving methods to explore the effects of fine-grain lumps or aggregates on the grain size distribution curves. The results demonstrate that the wet-sieve method results in finer particles than the dry-sieve, verifying that fine-grain clumps or aggregates may be generated during the drying process. Some clumps or aggregates may be crushed into smaller particles during sieving, but some remain. As shown in Fig. 1(b), soil aggregates and clumps affect the grain size distribution curve even though fines content ($d \leq 0.075$ mm) is less than 5% in both cases. In this experimental study, gravelly soils that were wet-sieved to separate the fine and coarse grains were used in testing to ensure a consistent grain size distribution. The soils classify as well-graded gravelly soils with a coefficient of uniformity C_u of approximately 42, have a specific gravity $G_s = 2.62$, a mean grain size $d_{50} = 4.5$ mm, a maximum

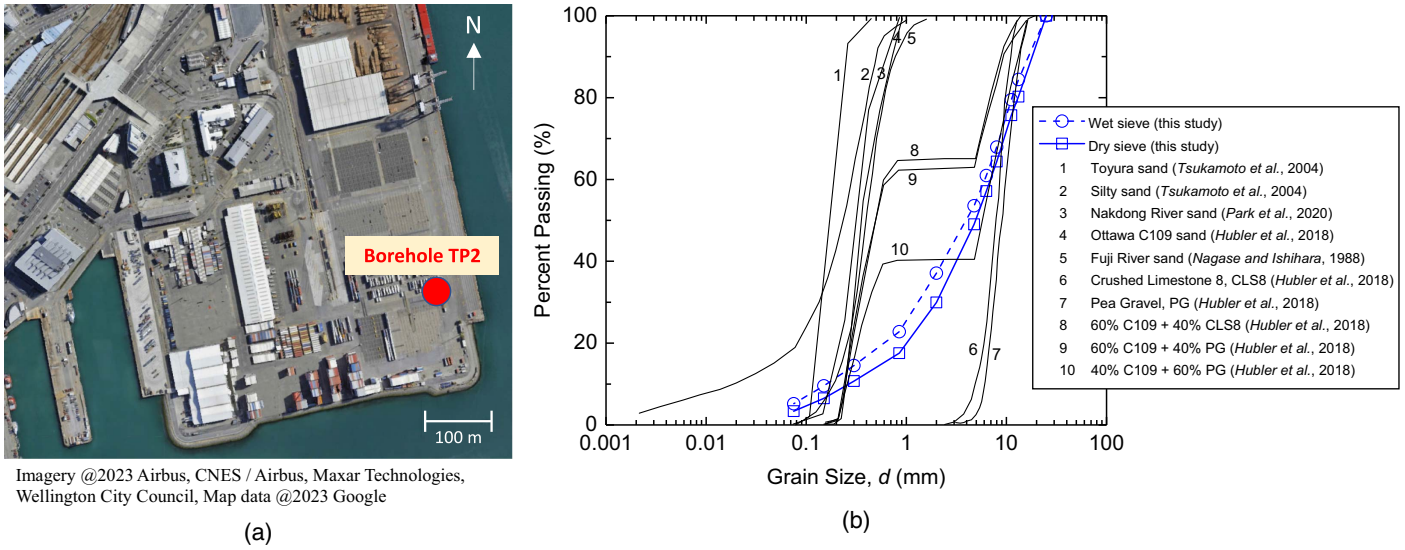

Fig. 1. Description of the tested well-graded sandy gravel soils obtained from CentrePort, Wellington, New Zealand: (a) satellite photo of CentrePort viewing the location of borings (Borehole TP2) (imagery ©2023 Airbus, CNES/Airbus, Maxar Technologies, Wellington City Council, map data ©2023 Google); and (b) grain size distribution of the well-graded sandy gravel analyzed using dry-sieve and wet-sieve methods (lines with markers) with comparison other soils from previous studies (solid lines).

J. Geotech. Geoenviron. Eng., 2023, 149(7): 04023046

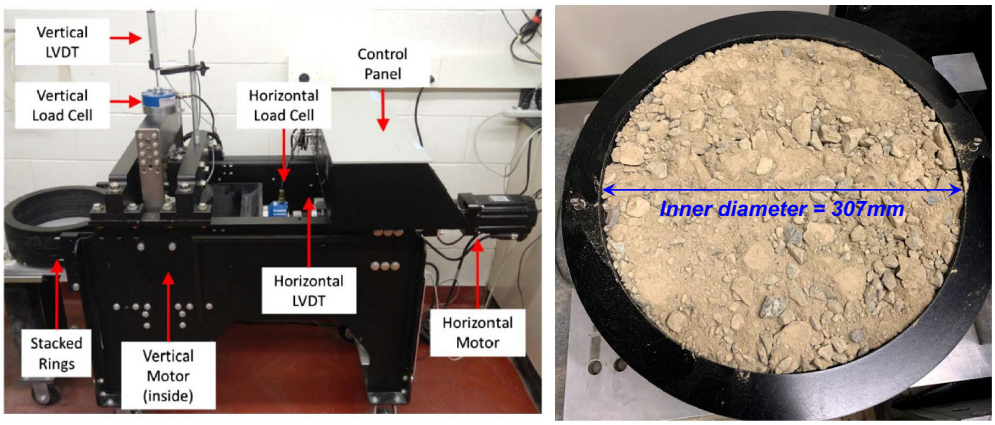

Fig. 2. (a) Experimental device, large scale monotonic and cyclic simple shear described in the previous study (reprinted from Hubler et al. 2017, © ASCE); and (b) prepared specimen inside the stack rings with an inner diameter of 307 mm.

void ratio $e_{max} = 0.568$, a minimum void ratio $e_{min} = 0.258$, and corresponding maximum and minimum dry densities $\gamma_{d,max} = 2{,}082$ and $\gamma_{d,min} = 1{,}671$ kg/cm^3, respectively. e_{max} and e_{min} were determined by placing the sand-gravel mixtures into a compaction mold as recommended in ASTM D4254-00 (ASTM 2006) and ASTM D698-12e2 (ASTM 2012) with a diameter of 152.4 mm. For e_{min} determination, the mixtures were placed into three layers, and each layer received an average of 25 tamps with a rubber mallet and a following 100 tamps with a 3-in-diameter steel cylinder. No particle segregation was observed during compaction. This method was validated in previous research by Hubler et al. (2017), who compared this method to the prediction method proposed by Fragaszy et al. (1990) for gap-graded gravel-sand mixtures. e_{max} was determined by placing the mixtures as loose as possible using a funnel at zero drop height to minimize particle segregation. Additional details of e_{max} and e_{min} determination for sand-gravel mixtures are described in Hubler et al. (2017). Note that similar values for e_{max} and e_{min} were obtained at the University of Canterbury, Christchurch, New Zealand, by using the Japanese method for the minimum and maximum density of gravels, JGS 1521-2003 (JGS 2003). These values are consistent with e_{max} and e_{min} values of gravels, and somewhat lower than reported values for gravel-sand-silt mixtures (Cubrinovski and Ishihara 2002).

Experimental Device

Fig. 2 depicts a large-scale cyclic simple shear (CSS) device used to perform monotonic and cyclic tests on the gravelly soils. The device allows the monotonic and cyclic simple shear testing of sandy gravel mixtures with a nominal diameter of 307 mm and a maximum height of 137 mm (Zekkos et al. 2018). The specimen is prepared inside a stack of 18 shear rings coated with tetrafluoroethylene (TFE)-fluoridation to minimize friction between them. These rings provide a constraint for lateral displacement during consolidation (i.e., K_0 condition) and facilitate shearing. The CSS device is equipped with vertical and horizontal load cells [maximum load capacity of 44,000 N (10,000 lbf) and 22,000 N (5,000 lbf), respectively] and linear variable differential transformers (LVDT) to monitor the vertical and horizontal displacements. The vertical and horizontal servomotors allow performance of the stress- and strain-controlled monotonic or cyclic simple shear tests. In addition, the monotonic and cyclic shear tests can be conducted under a constant volume or constant load conditions. Further details of the CSS device are described in Zekkos et al. (2018).

A pair of Micro-Electro-Mechanical Systems (MEMS) accelerometers mounted at the top and bottom caps are used to estimate the shear wave velocity of each specimen. A soft impulse is applied to the bottom cap, and first arrival time differences are calculated from the two accelerometers, as shown in Fig. 3. Each measurement provides the travel time of the shear wave propagating through the specimens. The captured shear wave signatures have a 195 kHz sampling frequency that corresponds to 5 μs time resolutions. Repeatability tests indicate that the calculated shear wave velocity may have up to an approximately 5% error associated with uncertainty in selecting the first arrival of the wave. This shear wave velocity measurement system has been validated on uniform gravel specimens by comparing the measurements of the MEMS accelerometer system to measurements using bender elements in the same CSS device (Hubler et al. 2017).

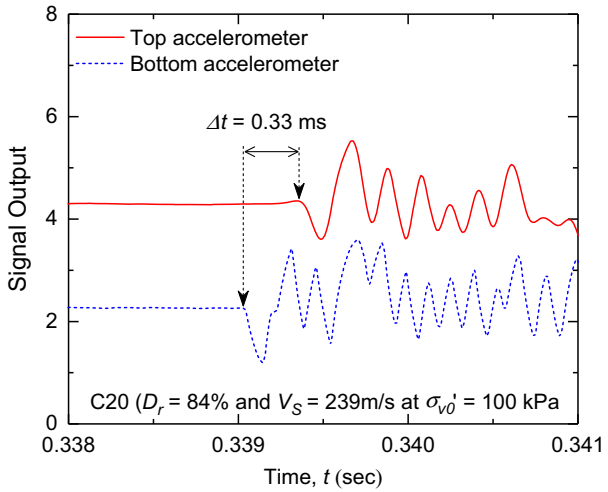

Fig. 3. Typical shear wave signatures measured from the bottom and top accelerometers. The signatures are captured from C20 specimens at $\sigma'_{v0} = 100$ kPa. Two arrows indicate the first arrival of the signatures, and Δt is used to calculate the shear wave velocity.

J. Geotech. Geoenviron. Eng., 2023, 149(7): 04023046

Experimental Study

Specimen Preparation

To prepare a specimen, the soil samples were screened using a No. 4 sieve (opening size = 4.75 mm) and then divided into two groups (i.e., sand and gravel) according to USCS. In this study, the sand/fines and gravel were mixed with a mass percentage of 49% and 51%, respectively, consistent with the field conditions [as shown in Fig. 1(b)]. Note that the prepared specimens have an approximately 5% fines content ($d < 0.075$ mm). ASTM D6528-07 (ASTM 2007) recommends that the maximum particle size does not exceed one-tenth of the specimen height in simple shear testing. The maximum gravel grain size in this study was limited to less than 25.4 mm to eliminate any potential oversize particle effects. In fact, more than 80% of the tested materials had a particle size less than 11 mm, as shown in Fig. 1(b). Therefore, a limited number of oversize particles (11 mm $< d <$ 25.4 mm) were included in the tested materials.

Specimens were prepared in dry condition with a diameter of 307 mm and a target as-prepared height of 115 mm. The sandy gravel mixtures with the predetermined mass ratio of sand and gravel were placed into the shear rings in three layers. The mixtures were uniformly placed to minimize particle segregation for the loose specimens, while compaction on each layer with a circular plate was adapted for the medium and dense specimens to achieve uniform density. Eventually, each layer had an identical amount of sand and gravel. Then, the specimens were subjected to an initial vertical effective stress $\sigma'_{v0} = 100$ or 400 kPa. The target relative densities D_r under $\sigma'_v = 100$ kPa were approximately 45% ± 5% (loosely packed), 65% ± 5% (medium packed), and 85% ± 4% (densely packed) for all tests. The target D_r at $\sigma'_{v0} = 100$ kPa was achieved by adjusting the mass and the initial height of the specimen before applying σ'_{v0}. No significant particle segregation was visually observed for any specimens before or after the test. A summary of the test conditions is provided in Table 1.

Table 1. Summary of test conditions

	At $\sigma'_{v0} = 100$ kPa or 400 kPa					Cyclic simple shear				Postcyclic tests ID		
Test ID	σ'_{v0}	Ms (kg)	γ_d kg/m^3	D_r (%)	V_S (m/s)	CSR	N_C	r_u	Liquefied	Reconsolidation	Postcyclic monotonic	Postcyclic reconsolidated monotonic
C01	100	14.9	1,817	41	195	0.15	4	0.97	O	PR01	—	—
C02	100	14.9	1,832	44	207	0.07	—	0.59[a]	X	PR02	—	—
C03	100	14.9	1,834	45	199	0.2	1	0.65	O	PR03	—	—
C04	100	14.9	1,828	44	199	0.085	60	0.96	O	PR04	—	—
C05	100	14.9	1,827	43	203	0.1	14	0.94	O	PR05	—	PRM05
C06	100	14.9	1,837	46	n/a	0.1	12	0.94	O	PR06	—	—
C07	100	14.9	1,839	46	194	0.1	—	0.91[a]	X	PR07	—	—
C08	100	14.9	1,834	47	196	0.1	—	0.82[a]	X	PR08	—	—
C09	100	14.9	1,843	47	195	0.1	17	0.96	O	PR09	—	—
C10	100	14.9	1,857	50	209	0.12	7	0.92	O	—	PM10	—
M01	100	14.9	1,850	49	207	—	—	—	X	—	—	—
C11	100	15.7	1,921	66	213	0.2	3	0.95	O	PR11	—	—
C12	100	15.7	1,921	66	219	0.1	64	0.98	O	PR12	—	—
C13	100	15.7	1,914	64	213	0.15	6	0.96	O	PR13	—	PRM13
C14	100	15.7	1,931	68	228	0.12	29	0.99	O	—	PM14	—
C15	100	15.7	1,912	64	219	0.085	197	0.99	O	—	PM15	—
C16	100	15.7	1,921	66	211	0.1	—	0.96[a]	X	PR16	—	—
C17	100	15.7	1,898	60	213	0.12	33	0.97	O	PR17	—	PRM17
C18	100	15.7	1,906	62	215	0.1	46	1.00	O	PR18	—	—
C19	100	15.7	1,926	67	206	0.1	45	1.00	O	PR19	—	—
M02	100	15.7	1,925	67	213	—	—	—	X	—	—	—
C20	100	16.8	2,001	84	239	0.1	67	0.99	O	—	PM20	—
C21	100	16.8	1,994	85	229	0.2	4	0.97	O	PR21	—	—
C22	100	16.8	2,004	84	235	0.12	43	0.98	O	PR22	—	PRM22
C23	100	16.8	2,028	89	246	0.1	89	0.99	O	PR23	—	—
C24	100	16.8	2,009	85	n/a	0.12	—	0.93[a]	X	PR24	—	—
C25	100	16.8	2,003	84	225	0.12	—	0.97[a]	X	PR25	—	—
C26	100	16.8	1,987	81	231	0.15	14	0.97	O	PR26	—	PRM26
C27	100	16.8	1,989	81	221	0.12	64	0.97	O	PR27	—	—
C28	100	16.8	2,007	85	224	0.2	6	0.97	O	PR28	—	—
C29	100	16.8	2,007	85	229	0.12	39	0.98	O	PR29	—	—
C30	100	16.8	2,010	85	224	0.12	37	0.98	O	PR30	—	—
M03	100	15.7	1,906	82	228	—	—	—	X	—	—	—
C31	400	15.0	1,914	64	276	0.15	2	0.86	O	PR31	—	—
C32	400	15.7	1,951	73	283	0.15	3	0.89	O	PR32	—	—
C33	400	16.8	2,035	91	293	0.15	7	0.92	O	PR33	—	—

Note: M_S = mass of specimen; γ_d = dry density; D_r = relative density; V_S = shear wave velocity; CSR = cyclic stress ratio; N_C = number of cycles at liquefaction; r_u = maximum excess pore water pressure ratio until shear strain reaches 3.75% single amplitude; PR = postcyclic reconsolidation; PM = postcyclic monotonic; and PRM = postcyclic reconsolidated monotonic.

[a]Indicates the maximum values during cyclic loading.

J. Geotech. Geoenviron. Eng., 2023, 149(7): 04023046

Experimental Procedures

A total of 33 specimens were prepared and subjected to a multistage testing sequence. First, specimens were subjected to K_0 consolidation up to 100 kPa vertical stress, then shear wave velocity measurements were conducted, followed by monotonic or cyclic simple shear. Cyclically tested specimens were subsequently subjected to either postcyclic reconsolidation or monotonic shear. Fig. 4(a) presents the relationship between D_r and V_S of the tested specimens measured at $\sigma'_{v0} = 100$ kPa, which is the stress state before applying monotonic or cyclic shear loading. The received wave signatures have an average frequency of 3 kHz, corresponding to the wavelength of 70–120 mm depending on the measured V_S, indicating that the wavelength is more than 10 times larger than $d_{50} = 4.5$ mm. Note that Zekkos et al. (2018) compared the velocities from bender elements and accelerometers and found them to be practically identical. The loosely packed specimens ($D_r \approx 45\% \pm 5\%$) have a V_S ranging from 194 to 209 m/s, whereas densely packed specimens ($D_r \approx 85\% \pm 4\%$) had a higher V_S, from 221 to 246 m/s. These V_S results are consistent with previous studies that predicted $V_S \approx 200$ m/s of well-graded sand-gravel mixtures ($D_r \approx 50\%$, $C_u = 13.1$) under isotropic confining stress $\sigma'_c = 98$ kPa (Hara et al. 2004). In Fig. 4(b), a relationship between the measured V_S and void ratio e is compared with the previous study (Kokusho and Yoshida 1997). Note that the overlapped V_{S1} of the previous study is the stress-corrected V_S calculated by the equation of $V_{S1} = V_S/[(\sigma'_v/P_0)(\sigma'_h/P_0)]^m$, where σ'_v and σ'_h is the vertical and horizontal effective stress, respectively; $P_0 = 98$ kPa is unit pressure; and m is assumed constant as 0.125. The study suggested that the V_S can generally be linearly related to e, with higher maximum V_S values at e_{min} as gravel content and C_u increase. As shown in Fig. 4(b), V_S of well-graded gravel with sand in this study is comparable to the previous results, but has somewhat of a flatter slope. It is noteworthy that the well-graded gravelly soils have a wider range in void ratio e and higher C_u than the poorly graded gravelly soils shown in Fig. 4(b).

In addition to the 33 specimens previously mentioned, three more specimens were prepared and subjected to $\sigma'_{v0} = 400$ kPa, and then cyclically sheared with an identical cyclic stress ration $(\text{CSR}) = 0.15$, followed by the postcyclic reconsolidation. V_s values were measured multiple times during the consolidation and reconsolidation phase after cyclic shear loading to evaluate the effects of liquefaction on V_s (and associated with effective stress reduction caused by the dynamic loading).

The monotonic and cyclic simple shear tests were performed on dry specimens under constant volume conditions considered equivalent to undrained conditions in a simple shear test, assuming that macroscopically, the changes in vertical effective stress correspond to excess pore water pressure (Dyvik et al. 1987). The constant volume condition was achieved during cyclic loading using an active feedback loop and restraint control of vertical cap movement. The results satisfy a recently proposed vertical strain criterion of 0.025% to ensure a fully undrained condition during cyclic loading (Basham et al. 2019), which is more stringent than the 0.05% recommended by ASTM for constant volume monotonic testing. The specimens were monotonically sheared up to a shear strain of 10% at a rate of 0.3% per min, which was similar to values used in simple shear testing of sands (Sivathayalan 2000). The cyclic simple shear test was conducted under stress-controlled conditions. Various CSRs, ranging from 0.07 to 0.2, were applied to estimate the liquefaction resistance. Cyclic loading was applied at frequency $f_r = 0.1$ Hz. The definition of liquefaction was the attainment of a single amplitude shear strain of 3.75%, a threshold that has been used in several previous studies (Hubler et al. 2017; Pillai and Stewart 1994; Porcino et al. 2008; Sivathayalan 2000; Vaid and Sivathayalan 1996).

Three types of postcyclic tests were conducted after the cyclic shear loading (summarized in Table 1): (1) postcyclic monotonic (PM) testing to assess the shear resistance of the material without excess pore water pressure dissipation (i.e., following reduction of vertical stress during a constant volume cyclic test); (2) postcyclic reconsolidation (PR) simulates the dissipation process of excess pore water pressure generated during the cyclic loading and provides an estimate of postcyclic volumetric strain; and (3) postcyclic reconsolidation monotonic (PRM) is the monotonic shear resistance following the full recovery of vertical effective stress (full dissipation of excess pore water pressure). Assessment of postcyclic undrained shear stress–strain response through PM and PRM tests provides the shear resistance of liquefied soils to support the following postcyclic monotonic loading.

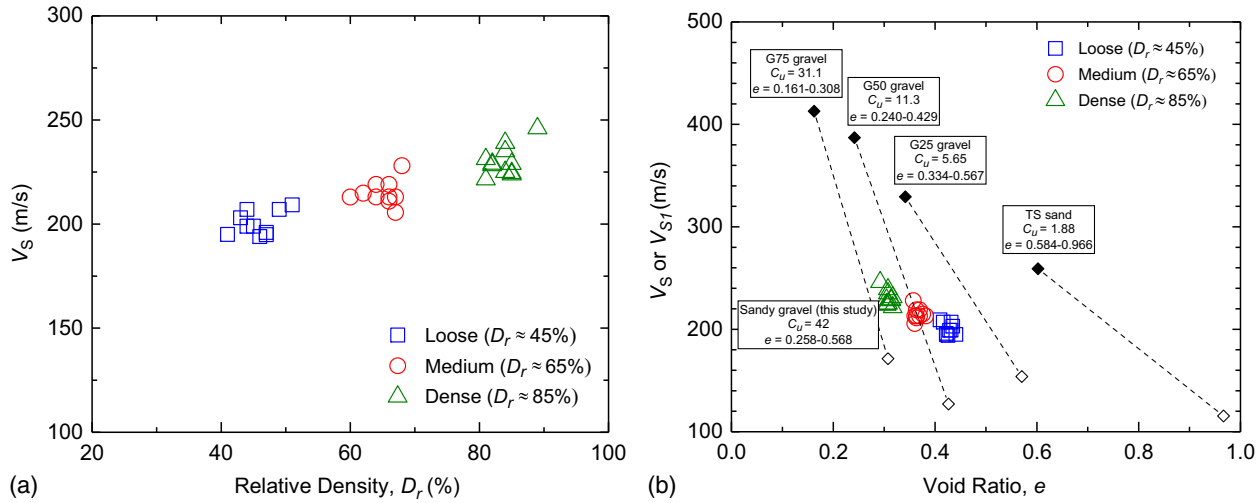

Fig. 4. Measured shear wave velocity V_S of well-graded sandy gravel specimens. V_S values are measured at $\sigma'_{v0} = 100$ kPa before monotonic or cyclic loading: (a) V_S versus relative density D_r; and (b) V_S versus void ratio e. Comparison with sand and sand-gravel mixtures from previous study was included. The range of void ratio e presented in the inset box indicates the e_{min} and e_{max} of soils. (Data from Kokusho and Yoshida 1997.)

Experimental Results

Monotonic Shear Response

Monotonic shear tests were performed on the sandy gravel mixtures at various relative densities D_r. Following the end of vertical stress ($\sigma'_{v0} = 100$ kPa), the specimens were monotonically sheared, and the relationships between normalized shear stress τ/σ'_{v0}, normalized vertical effective stress σ'_v/σ'_{v0}, and shear strain γ, as well as the corresponding stress paths, are presented in Fig. 5. It is noted that the fluctuation in shear stress and vertical effective stress observed near the shear strain of 4%–8% were possibly caused by the relatively large particle rearrangement during the cyclic simple shear under constant volume. This response is more pronounced for denser specimens, and is attributed to the active feedback loop and control of vertical strain. As shown in Fig. 5, higher shear strength is observed at higher relative density. The loose specimen M01 had a slight contractive tendency after the peak shear stress. For comparison, uniform and gap-graded gravelly specimens tested with $D_r = 47\% \pm 3\%$ and $\sigma'_{v0} = 100$ kPa (Hubler et al. 2018) are also shown in Fig. 5; and specifically the monotonic shear results of 100% C109 sand (dash line), 100% pea gravel (PG) (dot line), and 40% C109/60% PG mixtures (dash-dot line) that was considered the *optimum* mix of sand and gravel and had the maximum shear strength by Hubler et al. (2018). The grain size distribution of the tested materials is presented in Fig. 1(b). These results suggest that the uniformly graded specimens (i.e., 100% sand or 100% gravel) show a more contractive response than the well-graded gravelly soils tested in this study and exhibit a subsequent strain hardening at large shear strain (> approximately 3%) that was not observed in the well-graded soil. The gap-graded specimen, 40% C109/60% PG mixtures, also has a less contractive response and greater shear resistance compared to the well-graded specimen.

In contrast, medium dense (M02) and dense (M03) specimens, which showed no clear peak in shear stress, first exhibited contractive and then dilative response with continued increase in shear strain. Increasing packing density promoted more pronounced dilative behavior.

Cyclic Shear Response

Cyclic simple shear tests were performed on the gravelly soil prepared for the same relative densities to evaluate their liquefaction resistance. Details of the specimen conditions, including relative density D_r, initial vertical effective stress σ'_{v0}, and CSR, are summarized in Table 1. The typical undrained cyclic shear responses of the loose, medium, and dense specimens tested under identical conditions of $\sigma'_{v0} = 100$ kPa and CSR = 0.15 are depicted in Fig. 6.

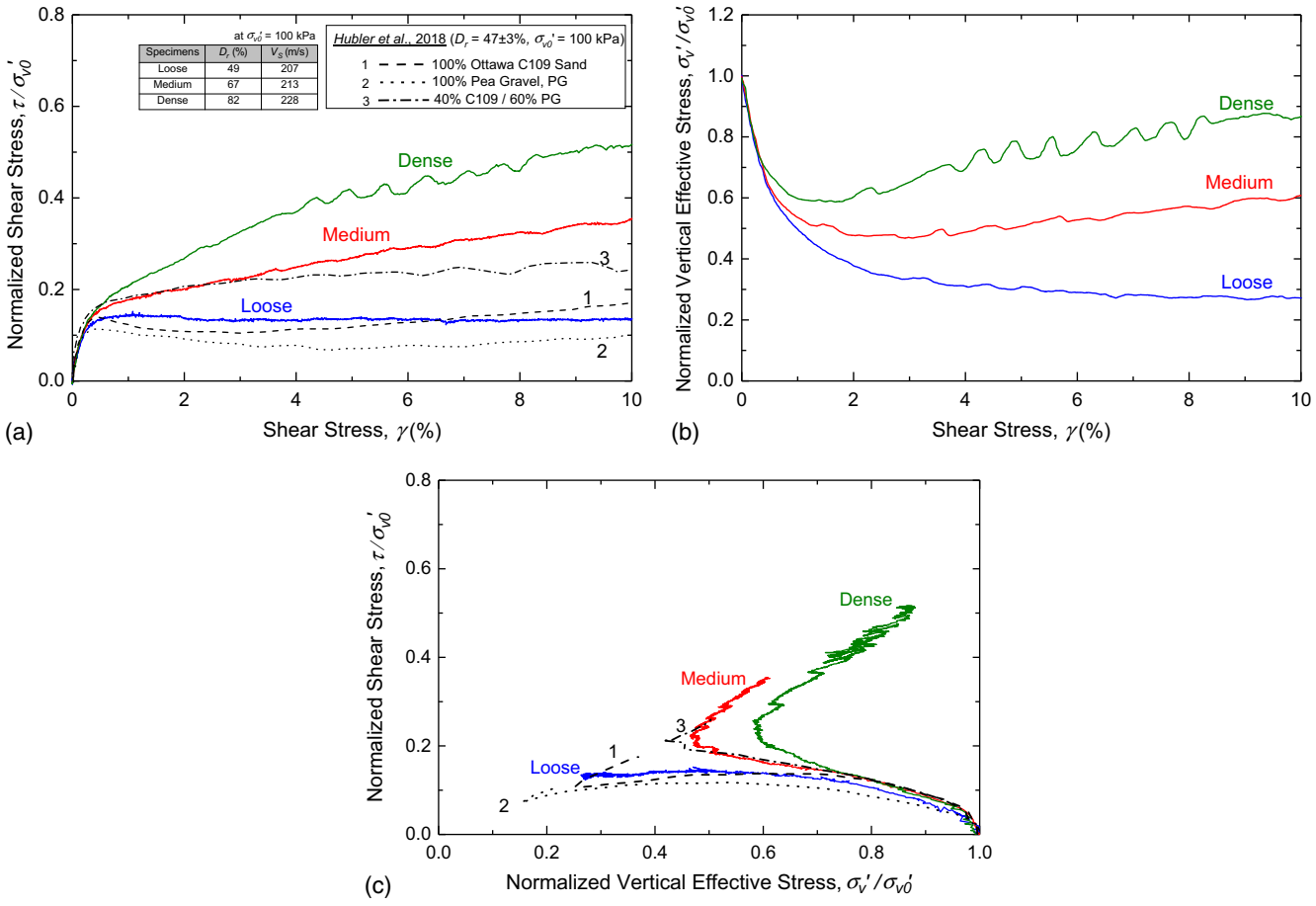

Fig. 5. Monotonic simple shear response of loose (M01), medium (M02), and dense (M03) packed specimens at $\sigma'_{v0} = 100$ kPa. The monotonic shear results of uniform Ottawa C109 sand (dashed line), uniform PG (dotted line), and gap-graded with 40% C109 and 60% PG (dash-dotted line) those were prepared with $D_r = 47\% \pm 3\%$ are included for the comparison with well-graded sandy gravel: (a) normalized shear stress τ/σ'_{v0} versus shear strain γ; (b) normalized vertical effective stress σ'_v/σ'_{v0} versus shear strain γ; and (c) normalized shear stress τ/σ'_{v0} versus normalized vertical effective stress σ'_v/σ'_{v0} up to shear strain of 10%. (Data from Hubler et al. 2018.)

J. Geotech. Geoenviron. Eng., 2023, 149(7): 04023046

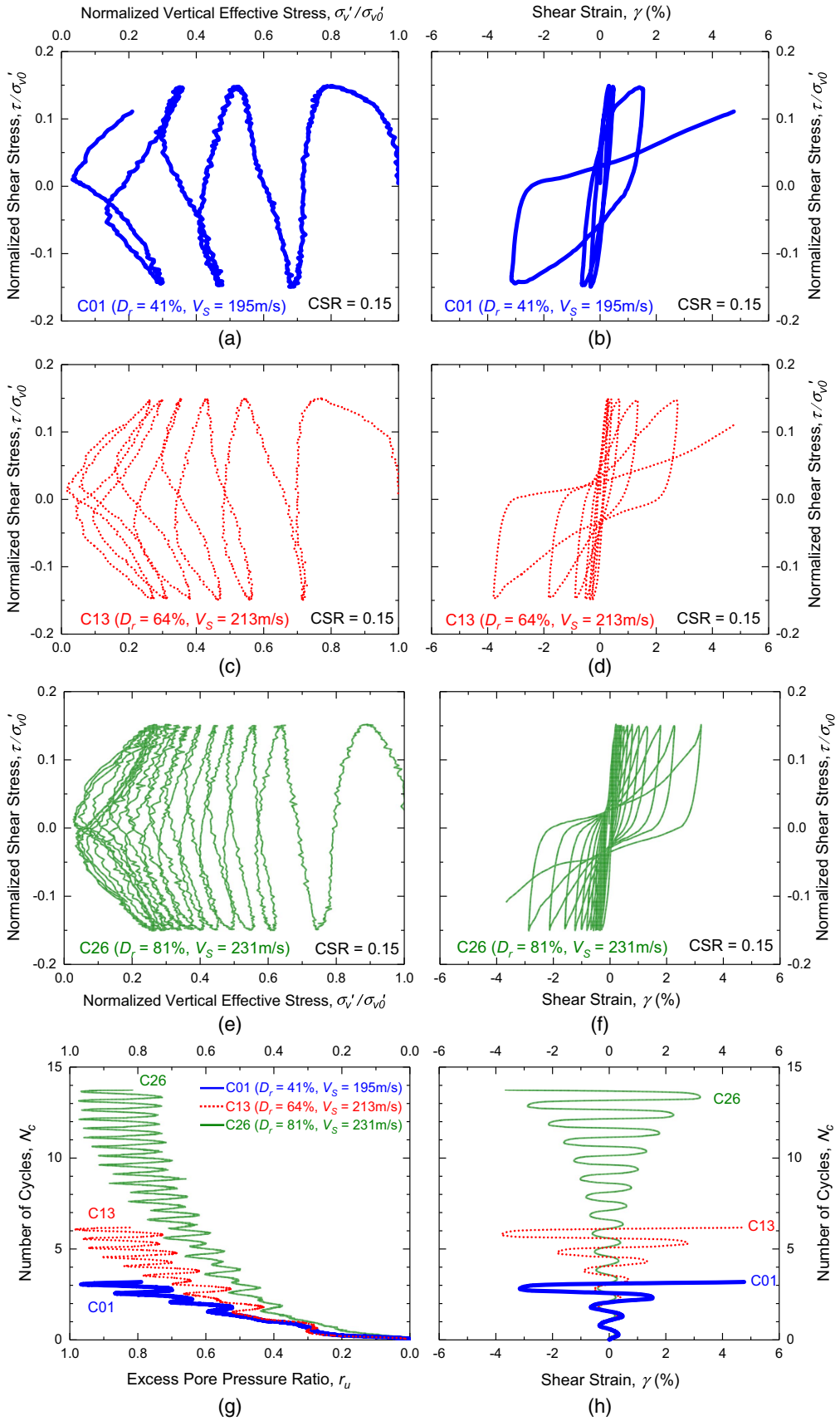

Fig. 6. Typical cyclic simple shear results of the loose (C01), medium (C13), and dense (C26) packed specimens. The specimens were consolidated to $\sigma'_{v0} = 100$ kPa and cyclically sheared with CSR $= 0.15$: (a) normalized vertical effective stress σ'_v/σ'_{v0} versus normalized shear stress τ/σ'_{v0} for loose specimen; (b) shear strain γ versus normalized shear stress τ/σ'_{v0} for loose specimen; (c) σ'_v/σ'_{v0} versus τ/σ'_{v0} for medium specimen; (d) γ versus τ/σ'_{v0} for medium specimen; (e) σ'_v/σ'_{v0} versus τ/σ'_{v0} for dense specimen; (f) γ versus τ/σ'_{v0} for dense specimen; (g) excess pore pressure ratio r_u versus number of cycles N_c for all specimens; and (h) shear strain γ versus number of cycles N_c for all specimens.

J. Geotech. Geoenviron. Eng., 2023, 149(7): 04023046

During cyclic testing, normalized vertical effective stress σ'_v/σ'_{v0} decreased from 1 and approached zero, due to a reduction in σ'_v. For the loosely packed specimen, the σ'_v/σ'_{v0} reduction was nearly continuous until the development of large strains. The medium and densely packed specimens showed a more pronounced reduction of σ'_v/σ'_{v0} within the first two or three cycles, and then a gradual reduction in σ'_v and shear strain γ accumulation was observed. The strain accumulation was slower in dense specimens, leading to a higher number of cycles N_c until liquefaction. These test results demonstrate a typical decrease in σ'_v due to cyclic shear loading causing a reduction of shear resistance and eventual liquefaction. The excess pore water pressure (represented by a change in vertical stress during a constant volume test) gradually increased as the cyclic loading progressed and finally approached close to σ'_{v0}, indicating the reduction of σ'_v to nearly zero under constant volume conditions.

Fig. 7(a) compares the relationship of CSR and N_c required to achieve 3.75% single amplitude shear strain. The results indicate that a greater N_c was required for the specimen with higher D_r, because the dense specimen exhibited less contractive behavior than the loose specimen, mainly associated with increased particle interlocking and a denser packing. In general, loosely packed specimens tend to contract during cyclic loading, while dense specimens tend to contract less or dilate during shearing, resulting in higher liquefaction resistance (Youd and Idriss 2001), similar to sandy soils (Cappellaro et al. 2021; Hubler et al. 2017; Monkul et al. 2015; Peacock and Seed 1968; Sivathayalan 1994; Vaid and Sivathayalan 1996; Vaid and Finn 1979). Similar behaviors were observed for this well-graded gravelly soils: denser specimens with less contractive behavior during the monotonic have higher liquefaction resistance than loosely packed specimens, and depending on the CSR, a large number of cycles is needed to reach liquefaction.

Fig. 7(b) compares the liquefaction resistance of various soils tested in the cyclic simple shear device in a loose packing condition ($D_r = 40\%$–47%) at $\sigma'_{v0} = 100$ kPa: the well-graded gravel with sand from Port of Wellington, New Zealand [Curve number 1 in Fig. 7(b)]; uniform sands, including angular Nakdong River sand (Curve number 2) (Park et al. 2020), and subrounded Ottawa C109 sand (Curve number 3) (Hubler et al. 2018); uniform gravel, including crushed limestone 8 CLS8 (Curve number 4) and subrounded PG (Curve number 5) (Hubler et al. 2018); and gap-graded sand-gravel mixtures of PG and CLS8 gravels and Ottawa C109 sand (Curve numbers 6–8) (Hubler et al. 2018). It is noted that Nakdong River sand (Park et al. 2020) was tested using a CSS device with a specimen diameter of 63.5 mm and a height of 25 mm, and all the other aforementioned materials were tested using the same large-scale CSS device described in this study. The grain size distribution of the materials is presented in Fig. 1(b). The angular Nakdong River sands show a higher liquefaction resistance than the other subrounded gravel, sands, and their mixtures, and this is mainly attributed to particle morphology (Hubler et al. 2018). Similar trends are also observed for the uniform gravel soils. Uniform angular CLS8 gravel shows a higher liquefaction resistance than the uniform subrounded PG gravel. The mixture of CLS8 and C109 (at optimum mass percentile 40% and 60%, respectively) shows a higher liquefaction resistance than the mixture of PG and C109. These results suggest that the liquefaction resistance of the gap-graded sand-gravel mixture is dominated by the applied CSR and proportions of sand and gravel. The well-graded gravelly soils tested in this study shows a similar or slightly higher liquefaction resistance than the gap-graded sand-gravel mixtures and uniform gravels. The well-graded gravelly specimens have a higher coefficient of uniformity $C_u = 42$ than other soils in Fig. 7(a). This comparison reinforces again that the liquefaction resistance is primarily affected by the particle morphology and size, soil fabric, packing density, coefficient of uniformity C_u, and CSR.

Postcyclic Response

Postcyclic Monotonic Tests

After completing the cyclic simple shear tests, the liquefied specimens were monotonically sheared, simulating the postcyclic monotonic PM test, without dissipating the excess pore water pressure generated during liquefaction. In all cases, the PM shear strain direction was opposite to the direction of the last cyclic loading and caused postcyclic shear stress reversal. Figs. 8(a and c) present normalized shear stress τ/σ'_{v0} and normalized vertical effective stress σ'_v/σ'_{v0} versus the shear strain of specimens with different

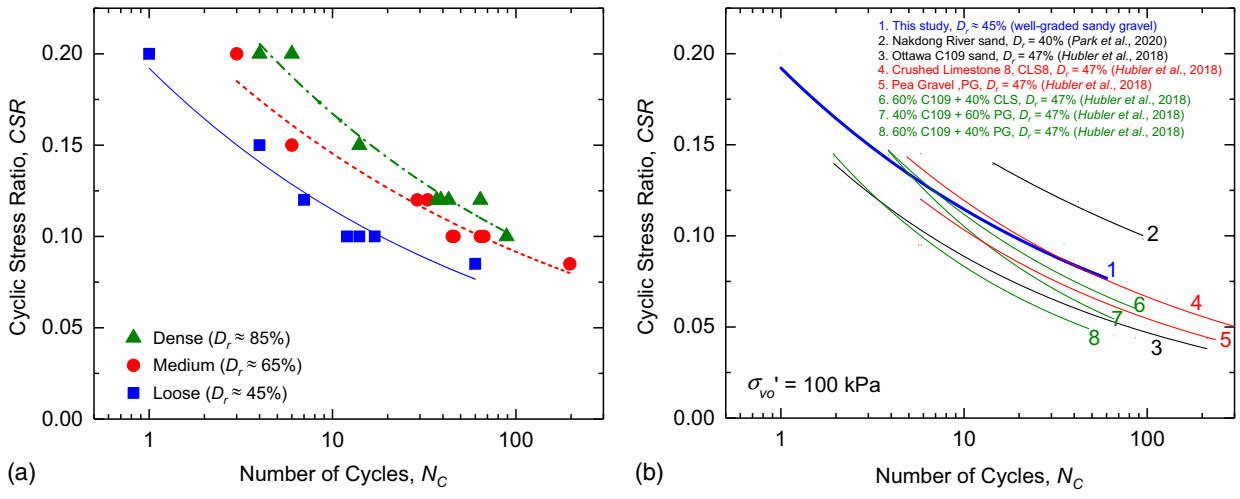

Fig. 7. CSR versus number of cycles N_c. The N_c is determined when the shear strain exceeds $\gamma = 3.75\%$ single amplitude or $\gamma = 7.5\%$ double amplitude: (a) specimens prepared with various relatively density D_r using well-graded sandy gravel obtained from Port of Wellington, New Zealand; and (b) comparison of liquefaction resistance of various soils, including uniform sand (Nakdong River sand and Ottawa C109 sand), uniform gravel (crushed limestone 8 CLS8 and PG), and gap-graded mixtures (CLS8 and PG with Ottawa C109 sands).

J. Geotech. Geoenviron. Eng., 2023, 149(7): 04023046

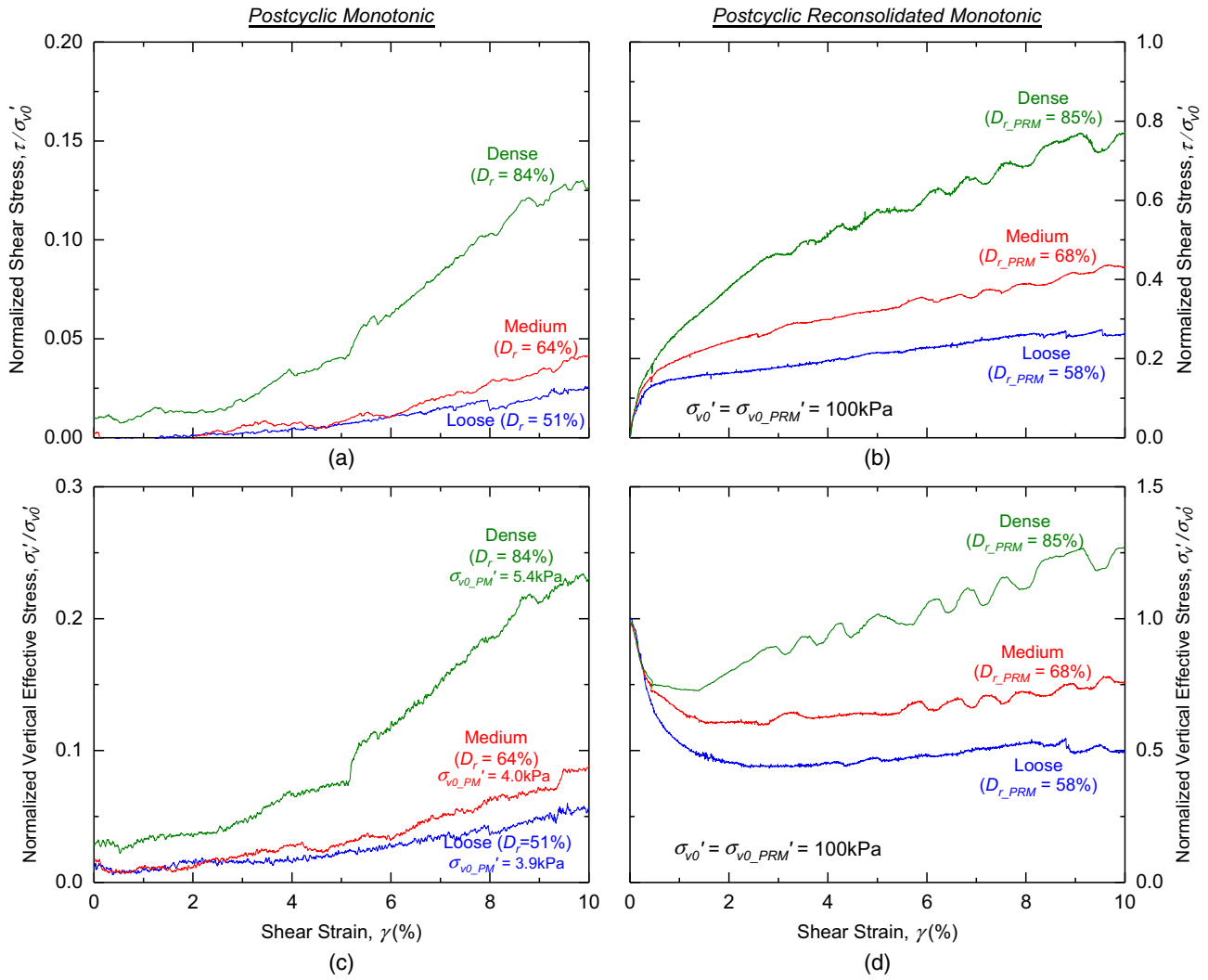

Fig. 8. PM and PRM responses of the liquefied specimens, including specimens with three different relative densities D_r (i.e., PM10 and PRM05 for loosely packing, PM15 and PRM17 for medium packing, and PM20 and PRM 26 for densely packing specimens): (a) normalized shear stress τ/σ'_{v0} versus shear strain γ for PM specimens; (b) normalized shear stress τ/σ'_{v0} versus shear strain γ for PRM specimens; (c) normalized vertical effective stress σ'_v/σ'_{v0} versus shear strain γ for PM specimens; and (d) normalized vertical effective stress versus σ'_v/σ'_{v0} shear strain γ for PRM specimens. σ'_{v0_PM} = vertical effective stress before postcyclic monotonic, and σ'_{v0_PRM} = vertical effective stress before postcyclic reconsolidated monotonic ($= \sigma'_{v0}$ in this study). Details of the specimens' properties are summarized in Table 1.

D_r values. The liquefied specimens had an excess pore water pressure close to σ'_{v0}, indicating that the σ'_v immediately after liquefaction was negligible, resulting in negligible shear resistance or stiffness. The residual vertical effective stress σ'_{v0_PM} values of liquefied specimens measured before postcyclic monotonic are inset in Fig. 8(c). The shear and vertical effective stress were normalized by $\sigma'_{v0} = 100$ kPa, which is the initial vertical effective stress before the cyclic loading. For loose specimen PM10, the τ/σ'_{v0} started to increase with developing shear strain after exceeding a shear strain of 3%–4%. Nevertheless, the increased rate (stiffness) was relatively small at the early shear strain development (<3%–4%) stage compared to the monotonic test without preceding cyclic loading (see Fig. 5). As shown in Fig. 8(c), the σ'_v/σ'_{v0} of the postcyclic monotonic, representing the changes in excess pore water pressure, slowly increased. Such a slow increase in σ'_v can be further evidence of lower shear stress development in the PM tests than in the virgin monotonic (M) tests. It was also found that a larger shear strain was required to initiate the recovery of the τ/σ'_{v0} for the loosely packed specimens.

Similar behavior has been observed for clean sands (Kokusho et al. 2004; Sitharam et al. 2009; Vaid and Thomas 1995) and sand-silt mixtures (Enomoto 2019). Postcyclic monotonic behavior observed in previous studies can be categorized into three phases. The liquefied specimen behaves like fluid in the first phase because of the fully developed excess pore water pressure (i.e., no effective stress). As the shear strain increases, in the second phase, the excess pore water pressure accumulated during the cyclic loading is reduced due to dilation of the soil (at a relatively high rate for dense soil and low rate for loose soil), and consequently the effective stress increases. In the last phase, the specimen dilates at a constant rate with the increase of shear strain.

The specimens with higher D_r showed higher PM shear stress after cyclic loading, similar to previous studies on sand (Sivathayalan 1994). At a shear strain of 10%, the gained τ/σ'_{v0} of the liquefied specimens during the PM test was lower than that found in the virgin monotonic shear test. The values of τ/σ'_{v0} during PM at 10% shear strain were 0.025, 0.04, and 0.125 for loose, medium, and dense specimens, respectively, showing 81%, 89%,

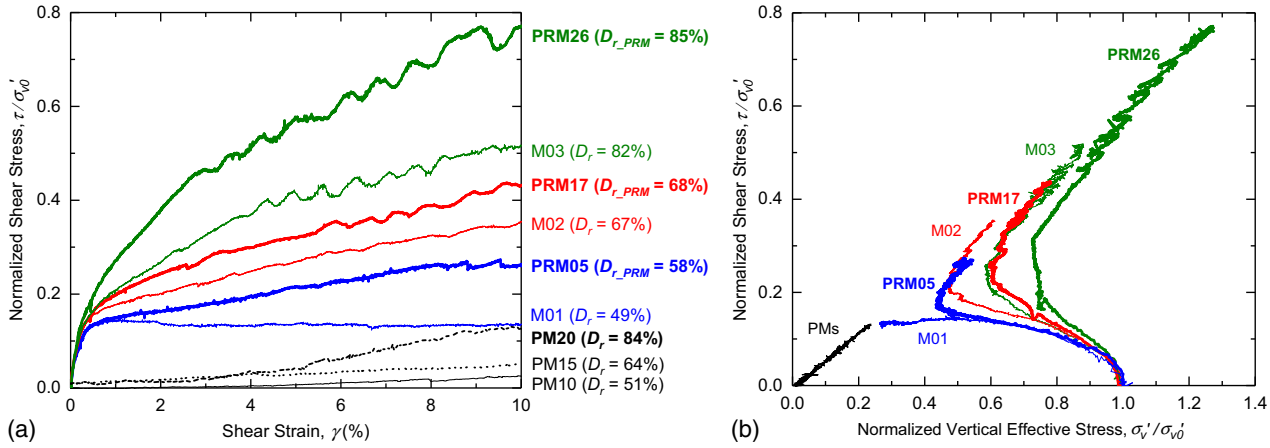

Fig. 9. Comparison of monotonic simple shear response for virgin M, PM, and PRM: (a) stress–strain response (normalized shear stress τ/σ'_{v0} versus shear strain γ); and (b) stress path response (normalized shear stress τ/σ'_{v0} versus normalized vertical effective stress σ'_v/σ'_{v0}). Black lines indicate the response of PM specimens, and rescaled data is available in Fig. 8(a). $D_{r-PRM'}$ = relative density after postcyclic reconsolidation. Details of the specimens' properties are summarized in Table 1.

and 76% reductions from the virgin monotonic results. These relatively lower τ/σ'_{v0} values can be attributed to the slow increase of shear stress immediately after liquefaction due to the lack of vertical effective stress. The results suggest that substantial shear strain is required to initiate or regain the postcyclic monotonic shear resistance. Note that σ'_v prior to the monotonic test of PM specimens are lower than those of M and PRM specimens due to excess pore water pressure generation and lack of reconsolidation.

Postcyclic Reconsolidated Monotonic Tests

Figs. 8(b and d) display the postcyclic reconsolidated monotonic PRM responses of the specimens with three different D_r values. The specimens that liquefied during the cyclic loading were recentered to have practically zero residual shear strain, followed by small shear strain adjustment (<0.001% shear strain) to zero the shear stress. Then, the specimens were reconsolidated to $\sigma'_{v0} = \sigma'_{v0\_PRM} = 100$ kPa. This process corresponded to the full dissipation of excess pore water pressure generated during liquefaction. Compared to the results from the PM in Figs. 8(a and c), the τ/σ'_{v0} of the PRM specimens increased immediately with the increase in shear strain. It can be seen that τ/σ'_{v0} gradually increases with an increase in shear strain, but the rate of increase of shear stress (i.e., stiffness) decreases, as in the results of the virgin monotonic tests. It is also interesting to note that the shear stress of PRM specimens was higher for all the shear strain ranges than the shear stress of the virgin monotonic specimens presented in Fig. 5(a). This can be attributed to the densification caused by the postcyclic reconsolidation, resulting in a stiffer soil fabric and skeleton before the postcyclic monotonic tests.

The results of σ'_v/σ'_{v0} in Fig. 8(d) show the sudden contractive response during shear. Then, the vertical effective stress σ'_v slightly recovered for the loose and medium density specimens as the shear strain increased. In contrast, the dense specimen showed a more pronounced recovery of σ'_v and eventually higher σ'_v than σ'_{v0}, resulting in higher undrained shear strength. Compared to the virgin monotonic response in Fig. 5(c), PRM specimens have a higher σ'_v/σ'_{v0} than M specimens. Reconsolidation of the liquefied specimens resulted in specimen compression to higher density. The details of the specimen densification effects caused by the postcyclic reconsolidation, including stress path, are discussed in the following analysis section.

Analyses and Discussion

Stress Path of Liquefied Specimens

Fig. 9 compares the monotonic shear response of a virgin M, PM, and PRM tests. D_r values of the specimens immediately before each monotonic shear test are also shown. The M and PM specimens had the same D_r throughout the various test stages because of the constant volume conditions of the monotonic and cyclic shear tests. In contrast, PRM specimens were denser due to reconsolidation after the cyclic loading.

As shown in Fig. 9(a) and Table 2, the M and particularly the PRM specimens with higher D_r had higher τ/σ'_{v0}. These results highlight that the updated D_r after the postcyclic reconsolidation significantly influences the undrained stress–strain response of PRM. In contrast, the relatively lower τ/σ'_{v0} of the PM specimens that have similar D_r values to the M specimens are primarily caused by the lower σ'_v following the cyclic induced liquefaction.

The stress path (i.e., the relationship between σ'_v/σ'_{v0} and τ/σ'_{v0}) is plotted in Fig. 9(b). It is observed that the M01 specimen

Table 2. Summary of virgin M, PM, and PRM

Test ID	D_r (%)	σ'_v (kPa)	τ (kPa)	τ/σ'_v	V_S (m/s)
M01	49	27.02	13.54	0.50	207
PRM05	43 (58$^+$)	49.11	25.66	0.52	203 (218$^+$)
PM10	51	9.69	4.65	0.48	209
M02	67	60.40	35.17	0.58	213
PRM13	64 (72$^+$)	129.11	78.47	0.61	213 (224$^+$)
PM14	68	42.96	24.13	0.56	228
PM15	64	8.87	4.15	0.47	219
PRM17	60 (68$^+$)	75.82	43.20	0.57	213 (228$^+$)
M03	82	86.55	51.69	0.60	228
PM20	84	22.86	12.72	0.56	239
PRM22	84 (90$^+$)	93.87	57.49	0.61	235 (244$^+$)
PRM26	81 (85$^+$)	127.2	77.16	0.61	231 (241$^+$)

Note: D_r = relative density; σ'_v = vertical effective stress at 10% shear strain γ; τ = shear stress at 10% shear strain γ; V_S = shear wave velocity; and $^+$ indicates the values of D_r or V_S for PRM specimens after postcyclic reconsolidation (= before postcyclic reconsolidated monotonic).

J. Geotech. Geoenviron. Eng., 2023, 149(7): 04023046

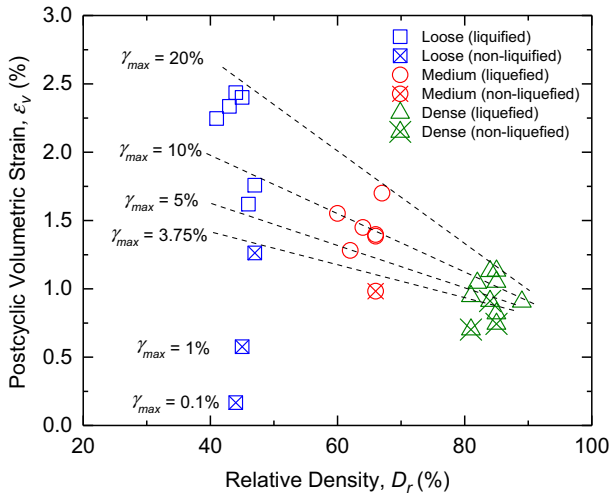

Fig. 10. Effects of relative density D_r on the postcyclic volumetric strain ε_v during PR. Both liquefied (empty markers) and nonliquefied (markers with a cross inside) specimens are presented. The maximum shear strain γ_{max} represents the single amplitude of the shear strain. The inset lines arbitrarily grouped the results according to the maximum shear strain during the cyclic loading.

(the only one at loose packing and monotonically sheared before cyclic testing) showed a continued contractive response, while the other M specimens exhibited a contractive followed by a dilative response as the shear strain increased due to higher D_r. Comparing the stress path of M, PM, and PRM specimens in Fig. 9(b), it is also interesting to note that they have practically the same ultimate strength line, which is independent of the stress histories, such as cyclic loading or postcyclic reconsolidation. Note that because the PRM specimens experienced further compression during reconsolidation, the contractive behavior during subsequent postcyclic monotonic tests is reduced compared to the M specimens.

Postcyclic Volumetric Strain

Postcyclic reconsolidation PR tests were conducted to assess postliquefaction volumetric compression due to the increase in vertical effective stress following the built-up of excess pore water pressure during cyclic loading. For this investigation, the cyclic loading process was intentionally terminated when the shear strain reached up to 20% to verify the effects of the maximum shear strain on the postcyclic volumetric strain. The specimens after cyclic loading were recentered to zero shear stress and shear strain. Then, the initial vertical stress of $\sigma'_{v0} = 100$ kPa was reapplied to the specimens. This section describes a comprehensive analysis and discussion on the postcyclic volumetric strain and the factors affecting it.

Effect of Relative Density

The relationship between postcyclic volumetric strain and D_r is illustrated in Fig. 10, including liquefied and nonliquefied specimens. D_r here is defined as the relative density immediately prior to cyclic shear testing. Fig. 10 demonstrates that the postcyclic volumetric strain of the liquefied gravel specimens (i.e., those with maximum shear strain over 3.75% single amplitude) decreased with an increase in relative density. This is due to the more pronounced contractive behavior of loosely packed specimens after cyclic loading. Also, liquefied specimens showed a greater postcyclic volumetric strain than nonliquefied specimens regardless of the D_r. The nonliquefied condition here is attained by applying smaller CSR values so as not to induce liquefaction or by intentionally terminating the cyclic loading at a shear strain before the liquefaction criteria of 3.75% single amplitude is met. The influence of the maximum shear strain during cyclic loading on the postcyclic volumetric strain is shown in Fig. 10 with indicative linear trends. Further analyses associated with the effects of the maximum shear strain are described in the following section.

Effect of the Maximum Shear Strain during Cyclic Shear Loading

The relationship between the maximum shear strain caused by the cyclic loading and the subsequent volumetric strain following reconsolidation is summarized in Fig. 11(a). It is interesting to note

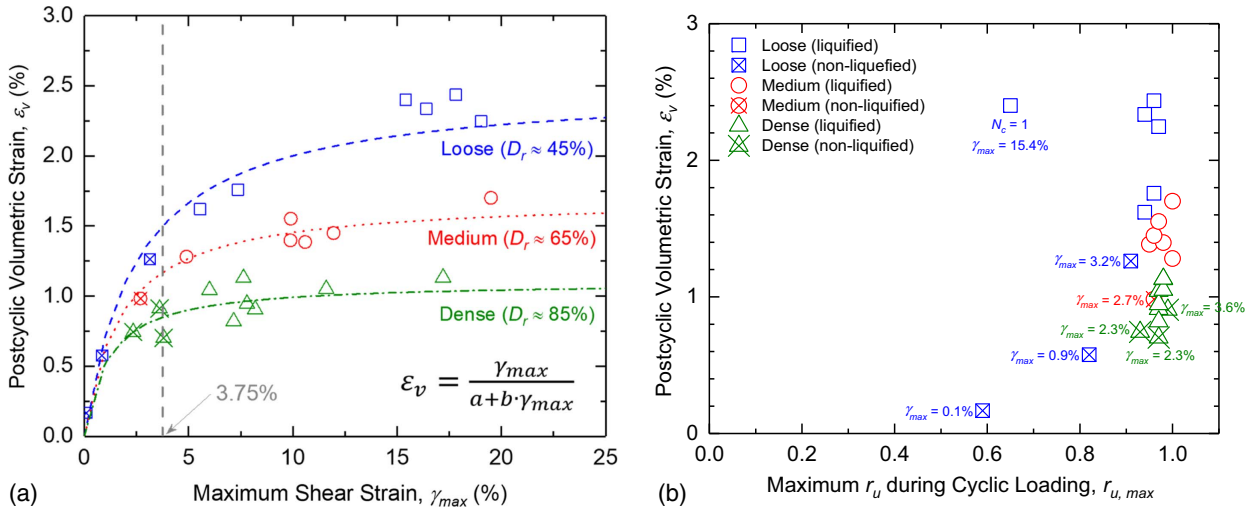

Fig. 11. Effects of the maximum shear strain γ_{max} and maximum pore pressure ratio during cyclic loading $r_{u,max}$ on the volumetric strain ε_v during the PR: (a) effects of the γ_{max}; and (b) effects of $r_{u,max}$. The vertical reference bar indicates $\gamma = 3.75\%$ (single amplitude) as the liquefaction criteria used in this study; dashed curves estimate the ε_v using the hyperbolic model in Eq. (1); maximum shear strain values of nonliquefied specimens during cyclic loading were presented; and both liquefied (empty markers) and nonliquefied (markers with a cross inside) specimens are presented.

J. Geotech. Geoenviron. Eng., 2023, 149(7): 04023046

that higher maximum shear strain during cyclic testing results in higher volumetric strain, with the maximum volumetric strain reaching a plateau when the maximum cyclic shear strain was larger than ~7%–15%, with loosely packed specimens reaching higher volumetric strains than densely packed specimens. Higher maximum shear strain is also needed for the loose specimens to reach their ultimate postcyclic volumetric strain. The results were fitted with the proposed hyperbolic model as follows:

$$\varepsilon_v = \frac{\gamma_{max}}{a + b \cdot \gamma_{max}} \quad (1)$$

where ε_v = volumetric strain during postcyclic reconsolidation; γ_{max} = maximum cyclic shear strain experienced during cyclic loading; and a and b values are fitting parameters. The $1/a$ parameter describes the initial slope of the model, and $1/b$ affects the ultimate postcyclic volumetric strain of each specimen. The determined ultimate postcyclic volumetric strains ε_{v_ult} were 2.5% (loosely packed), 1.7% (medium packed), and 1.1% (densely packed); the corresponding b values were 0.4, 0.59, and 0.91, respectively. Although similar data for gravelly soils under simple shear do not exist; Nagase and Ishihara (1988) and Ishihara and Yoshimine (1992) performed an experimental study on Fuji River sand using a multidirectional cyclic simple shear device. They concluded that the volumetric strain during postcyclic reconsolidation is uniquely correlated with the developed excess pore water pressure only when the values are smaller than the initial applied vertical stress. They also proposed a bilinear relationship between maximum cyclic shear strain and the postcyclic volumetric strain on the river sand. Jana and Stuedlein (2021) and Wijewickreme et al. (2019) have shown correlations between postcyclic volumetric strain and excess pore pressure for fine-grained soils.

Fig. 11(b) presents the relation between the maximum pore water pressure ratio during the cyclic loading $r_{u,max}$ and postcyclic volumetric strain ε_v. The generated r_u in this study ranged from 0.94–1 when the specimen exceeded the shear strain criteria. The nonliquefied specimens also developed r_u over 0.9 except for the specimens that generated the low shear strain (i.e., $\gamma_{max} < 1\%$ for loose specimens). Even though $r_{u,max}$ values were over 0.9, the nonliquefied specimens that experienced the lower maximum shear strain showed the lower postcyclic volumetric strain. This study indicates that the degree of excess pore water pressure may not be an appropriate indicator to estimate the subsequent volumetric strain of the liquefied specimens (Ishihara et al. 2016; Ishihara and Yoshimine 1992; Karakan et al. 2019; Nagase and Ishihara 1988). For example, the specimen that liquefied at the first cycle had r_u of 0.65 with γ_{max} of 15.4% and had a similar postcyclic volumetric strain response to the specimens with full development of r_u (>0.94). Instead, as indicated by the hyperbolic model in Fig. 11(a), the maximum shear strain during cyclic loading appears to be an appropriate parameter to estimate postcyclic volumetric strain during the subsequent reconsolidation of the gravelly soils. Further comparison of postcyclic volumetric strain with other soils is discussed in the following section of "Comparison with Other Soils."

Effect of the Cyclic Stress Ratio

Fig. 12 illustrates the variation in ultimate postcyclic volumetric strain ε_{v_ult} with CSR of the liquefied specimens that experienced high enough maximum cyclic shear strain γ_{max} (i.e., >15% for loose, >10% for medium, and >7% for dense specimens) to constraint the γ_{max} effects. As also shown earlier, the loosely packed specimens showed a higher ultimate postcyclic volumetric strain, approximately 2.5%, than the densely packed specimens, which showed a volumetric strain of approximately 1.1%. However, CSR had no influence on the postcyclic volumetric strain when the specimens were cyclically sheared with a higher accumulated shear strain as aforementioned, indicating that the ultimate postcyclic volumetric strain of the liquefied specimens may be independent of cyclic stress ratio CSR. In contrast, D_r and the maximum shear strain during cyclic shear loading are the main factors influencing the postcyclic volumetric strain of the liquefied sandy gravel mixtures, as discussed in Figs. 10 and 11.

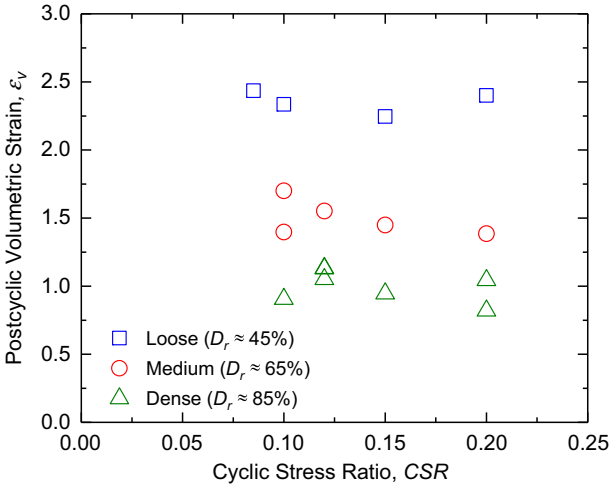

Fig. 12. Relation between CSR and volumetric strain ε_v during the PR. The postcyclic volumetric strain was only selected from the specimens that experienced high enough maximum cyclic shear strain γ_{max} (i.e., >15% for loose, >10% for medium, and >7% for dense specimens) to constraint the γ_{max} effects.

Comparison with Other Soils

Fig. 13 presents the effects of relative density D_r on the ultimate postcyclic volumetric strain ε_{v_ult} for the tested well-graded gravelly and other soils investigated by previous studies. It is noted that Fuji River sand was tested in a cyclic simple shear system at $\sigma'_{v0} =$ 196 kPa (Nagase and Ishihara 1988), whereas Toyoura sand and silty sand were tested in a triaxial system at an isotopic confining stress $\sigma'_0 = 98$ kPa (Tsukamoto et al. 2004). In Fig. 13, ε_{v_ult} represents values after reaching a strain plateau for each specimen (i.e., $\gamma_{max} \geq 10\%$, 6%, and 8% for Fuji River sand, Toyoura sand, and silty sand, respectively). Corresponding grain size distributions are presented in Fig. 1(b). All specimens in Fig. 13 show lower ε_{v_ult} with an increase in D_r, as discussed in Figs. 10 and 11. Comparing two types of clean sand, although Fuji River sand has a larger d_{50} than Toyoura sand in Fig. 1(b), the higher overburden stress may result in the higher ε_{v_ult} values in Fuji River sand (Lee and Albaisa 1974). ε_{v_ult} of silty sand is greater than clean sands and well-graded gravelly soils, and it is primarily attributed to the fine contents ($F_c = 19.6\%$, nonplastic) within the silty sand. Note that the F_c of the well-graded gravelly soils is approximately 5%. Similar responses were observed in both undisturbed and reconstituted specimens for clean sands and silty sands (Ishihara et al. 2016; Tsukamoto et al. 2004). It is also found that the well-graded gravelly soils show similar or slightly lower ε_{v_ult} values than Fuji River and Toyoura sands. Particularly in loose packing conditions ($D_r = 40\%$–45%), a much lower value in ε_{v_ult} is observed for the well-graded gravelly soils compared to the two clean sands. Many factors may affect the postcyclic volumetric strain response (i.e., particle size d, coefficient of uniformity C_u, overburden stress σ'_{v0} or σ'_v, fine contents F_c or gravel contents in gravelly soils,

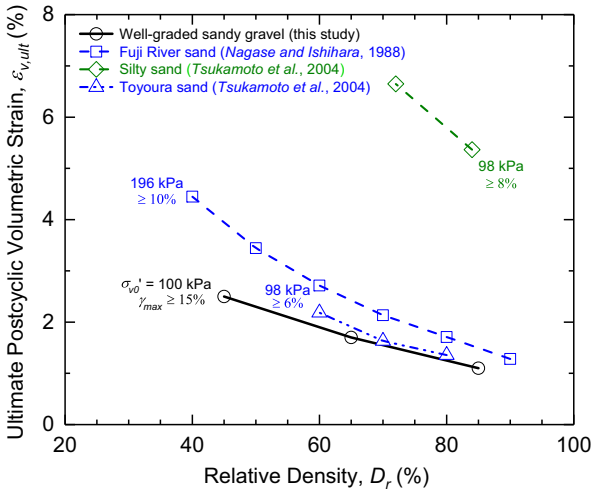

Fig. 13. Relation between the ultimate postcyclic volumetric strain ε_{v_ult} and relative density D_r. ε_{v_ult} values were captured at the maximum cyclic shear strain exceeded 15% [after the plateau in Fig. 11(b)]. The results of two sand and silty sand are included for comparison. The inset numbers indicate the postcyclic reconsolidation stress and the maximum cyclic shear strain. Note that silty sand and Toyoura sand were tested in a triaxial testing system (Tsukamoto et al. 2004), and Fuji River sand was tested in a simple shear system (Nagase and Ishihara 1988). Grain size distributions of the soil materials are presented in Fig. 1(b).

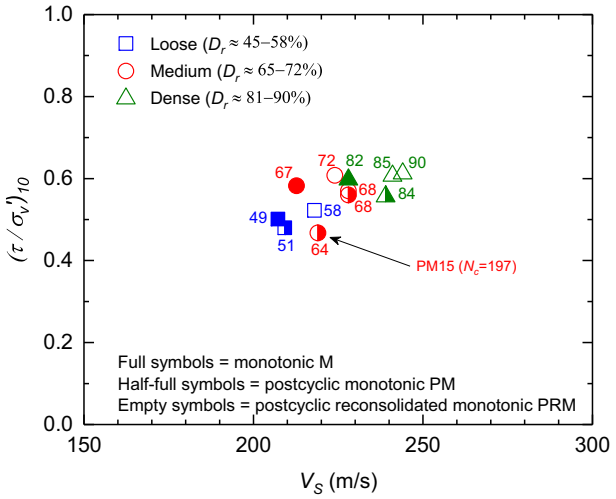

Fig. 14. Virgin and postcyclic monotonic shear stress ratio $[(\tau/\sigma'_v)_{10}]$ versus shear wave velocity V_S. $[(\tau/\sigma'_v)_{10}]$ represents the ratio of shear stress τ and vertical effective stress σ'_v at a shear strain of 10%. V_S values were measured at $\sigma'_{v0} = 100$ kPa after specimens' preparation for M and PM specimens, and at $\sigma'_{v0\_PRM} = 100$ kPa before postcyclic reconsolidated monotonic. Virgin M (full symbols), PM (half-full symbols), and PRM (empty symbols) are presented. Inset numbers represent D_r values for the monotonic tests and V_S measurements. Note that slightly higher D_r and V_S values of PRM specimens is attributed to the postcyclic reconsolidation. Corresponding values are summarized in Table 2.

relative density D_r, and maximum cyclic shear strain γ_{max}). Especially, gravelly soils with a higher coefficient of uniformity ($C_u = 13.1$) tend to have a higher liquefaction resistance than poorly graded sand ($C_u = 1.44$) in the triaxial system, and following postcyclic reconsolidation induces less postcyclic volumetric strain with the increase in C_u (Hara et al. 2004). Similarly, the well-graded gravelly soils ($C_u = 42$) tested in the simple shear system show a slightly lower postcyclic volumetric strain than poorly graded sand that typically has a larger void ratio. In addition, the void ratio range [i.e., $(e_{max} - e_{min})$] can be considered a measure of the soil deformation potential. The tested gravelly soils have a relatively lower void ratio range of 0.31 compared to the other soils presented in Figs. 4 and 13, such as TS sand = 0.382, Toyoura sand = 0.366, Fuji River sand = 0.535, and silty sand = 0.596, indicating the well-graded gravelly soils' limited capacity of volume change.

Normalized Shear Strength versus Shear Wave Velocity

Fig. 14 illustrates the relationship of $(\tau/\sigma'_v)_{10}$ from a monotonic shear test with shear wave velocity V_S of the M (full symbols), PM (half-full symbols), and PRM specimens (empty symbols). The shear stress τ at a shear strain of 10% is plotted herein and normalized with the corresponding vertical effective stress σ'_v. Note that the monotonic shear stress ratio has been preceded in some cases by cyclic shear loading (shown as half-filled and empty symbols), but not in other cases (shown as full symbols). V_S of the specimens was measured at $\sigma'_{v0} = 100$ kPa after specimens preparation for M and PM specimens, and at $\sigma'_{v0\_PM} = 100$ kPa before postcyclic reconsolidated monotonic. Particularly, the V_S values of PRM specimens were measured after postcyclic reconsolidation that caused densification and approximately 5% increase in V_S. Table 2 summarizes the monotonic test results (i.e., M, PM, and PRM specimens) with these values.

As shown in Fig. 14, higher V_S values were observed for dense specimens. The $(\tau/\sigma'_v)_{10}$ had a slightly increasing trend as V_S increased regardless of the test conditions, also observed in a previous study on pea gravel and crushed limestone (Hubler et al. 2017). It is noteworthy that the $(\tau/\sigma'_v)_{10}$ in the present study ranged from 0.48 to 0.61, and the variation mostly depends on the D_r. There was also a small but discernible difference in the $(\tau/\sigma'_v)_{10}$ depending on the test types (i.e., M, PM, and PRM). In the same D_r group, PRM specimens had the highest $(\tau/\sigma'_v)_{10}$, and PM specimens had the lowest values. This is mainly attributed to the densification during postcyclic reconsolidation of PRM specimens before being subjected to postcyclic reconsolidated monotonic. For PM specimens, a higher $(\tau/\sigma'_v)_{10}$ could be expected due to the lack of σ'_v. However, each PM and PRM specimen experienced a different amplitude of CSR and different levels of the maximum cyclic shear strain, as provided in Table 1. These variations may affect $(\tau/\sigma'_v)_{10}$ due to various degrees of specimen disturbance, resulting from particle arrangement, stiffness, and skeleton variations. Further investigation is recommended to estimate the effects of cyclic loading histories (i.e., CSR and the maximum cyclic shear strain) on the postcyclic monotonic response. However, at given ranges of CSR and maximum cyclic shear strain during the cyclic shearing, the results indicate that the variation of the $(\tau/\sigma'_v)_{10}$ is less than 10% in the same D_r group, except PM15 that experienced an extremely high number of cycles. It is also interesting to note that PM15 (with $N_c = 197$) had the lowest $(\tau/\sigma'_v)_{10}$, possibly indicating that high N_c can damage the specimen and weaken the shear stiffness and strength by altering the soil fabric and skeleton. These observations again support that the cyclic loading histories, which are highly related to the specimens' disturbance, play an important role in $(\tau/\sigma'_v)_{10}$. The results propose that D_r and σ'_v (closely related to excess pore water pressure generation and

dissipation) and high N_c (triggering significant soil fabric and skeleton changes) primarily affect the postcyclic normalized shear strength ratio. Furthermore, this relation provides the $(\tau/\sigma'_v)_{10}$ estimation of well-graded gravelly soils under various conditions (M, PM, and PRM) using V_S measured before the monotonic or postcyclic monotonic (i.e., M, PM, or PRM) conditions.

Change in Shear Wave Velocity before and after Liquefaction

A set of tests were performed to estimate the V_S before and after cyclic loading. The specimens were prepared to have a similar target D_r (≈45% for loose, 65% for medium, and 85% for dense specimens) at $\sigma'_v = 100$ kPa. However, the specimens were additionally subjected to $\sigma'_{v0} = 400$ kPa to obtain the specific relation of V_S and σ'_v. This higher σ'_{v0} induces higher D_r values than at $\sigma'_v =$ 100 kPa (i.e., 64% for loose, 73% for medium, and 91% for dense specimens at $\sigma'_{v0} = 400$ kPa). Then, cyclic shear loading with an identical CSR = 0.15 was applied to the specimens to trigger liquefaction, followed by postcyclic reconsolidation to $\sigma'_{v0} = 400$ kPa. The accelerometer time histories were captured at each loading step and were used to interpret V_S and evaluate the effects of liquefaction and subsequent postcyclic reconsolidation. Fig. 15 displays the calculated V_S during the loading process before cyclic loading (dash lines in Fig. 15) and during step-by-step dissipation of excess pore water pressure after liquefaction (solid lines in Fig. 15).

The V_S variation with vertical stress can be expressed by a Hertzian-type power model as follows:

$$V_s = \alpha\left(\frac{\sigma'_v}{1\ \text{kPa}}\right)^{\beta} \tag{2}$$

where α (m/s) = reference V_S at nominal vertical stress of 1 kPa; and β = exponent parameter expressing the sensitivity of V_S to σ'_v. Eq. (2) describes the variation of V_S with σ'_v, which is displayed in Fig. 15. Before liquefaction (dash lines in Fig. 15), dense specimens had a higher V_S than loose specimens at all σ'_v due to higher interparticle contacts, which resulted in higher α values. The dense specimens had slightly lower values of β, indicating a less pronounced influence of the σ'_v on the V_S as D_r increased (Santamarina et al. 2001). After liquefaction, the specimens were recentered for the postcyclic reconsolidation with no residual shear stress and shear strain. The measured V_S after recentering was lower than the values expected from the virgin consolidation (dash lines in Fig. 15), indicating that the liquefied specimens do not follow the V_S trend expected due to unloading [with overconsolidation ratio (OCR) > 1], and instead have an even lower small-strain stiffness than before liquefaction. During the postcyclic reconsolidation process, the V_S increased and reached slightly higher values than before liquefaction at the same vertical effective stress of 400 kPa. The V_S relationship with vertical stress at postliquefaction (solid lines in Fig. 15) displayed lower α and higher β values than before. The higher V_s values of the reconsolidated specimen may be attributed to the densification and fabric changes of the specimens during postcyclic reconsolidation, as discussed in Fig. 9. In fact, D_r after the postcyclic reconsolidation to $\sigma'_{v0} =$ 400 kPa increased from 64% to 71% for C31, from 73% to 81% for C32, and from 91% to 97% for C33. This suggests that a denser soil fabric and skeleton during reconsolidation plays a critical role in recovering soil stiffness weakened by previous cyclic loading.

Conclusions

This study experimentally investigated the monotonic and cyclic responses of well-graded gravel with sand collected from Centre-Port, Wellington, New Zealand, that liquefied during the 2016 Kaikoura earthquake. The specimens prepared at various D_r were tested under constant volume monotonic and cyclic simple shear conditions, including postcyclic responses: postcyclic volumetric strain, postcyclic monotonic, and postcyclic reconsolidated monotonic

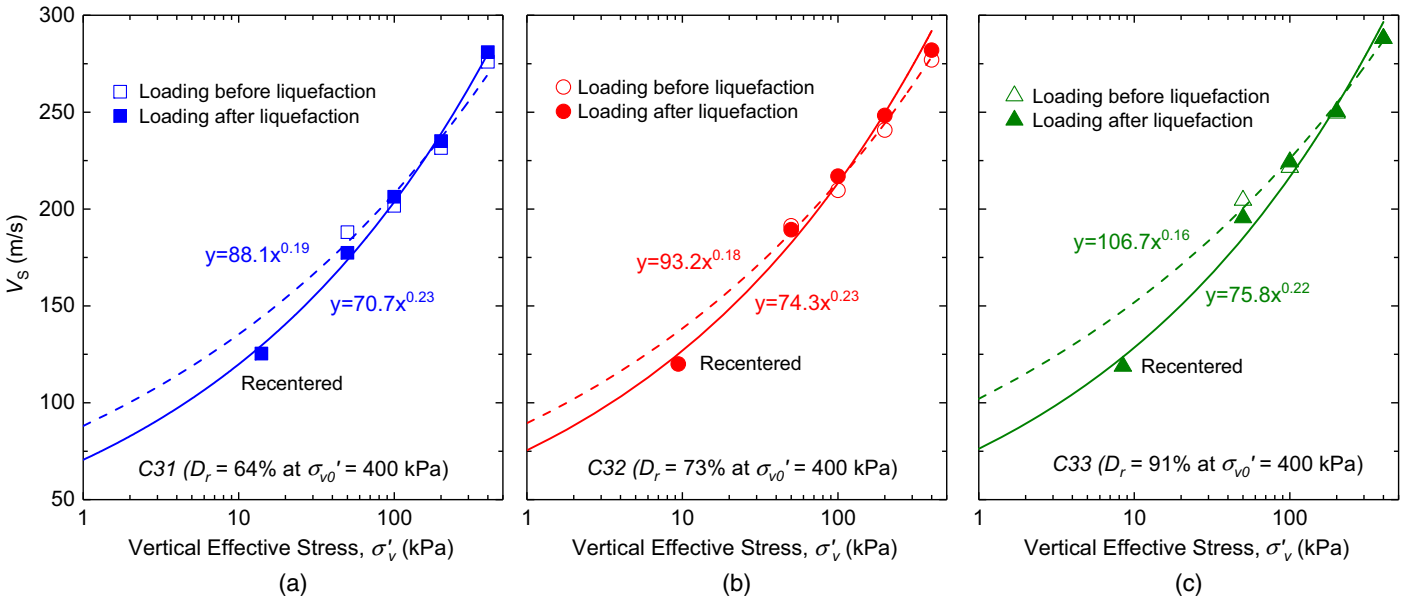

Fig. 15. The shear wave velocities V_S versus vertical effective stress σ'_v before and after the liquefaction: (a) loosely packed; (b) medium packed; and (c) densely packed. The specimens before the liquefaction were subjected to $\sigma'_{v0} = 400$ kPa (dash line with empty markers), and the liquefied specimens are recentered and reconsolidated to $\sigma'_{v0\_PRM} = \sigma'_{v0} = 400$ kPa (solid line with filled markers). Solid star markers indicate the status immediately after the liquefaction.

J. Geotech. Geoenviron. Eng., 2023, 149(7): 04023046

tests. Shear wave velocities were measured before and after liquefaction. The main conclusions from this study are:

- The sandy gravel soils have the potential for liquefaction even when the shear wave velocity V_S is higher than 200 m/s at the initial vertical effective stress $\sigma'_{v0} = 100$ kPa (up to approximately 246 m/s for $D_r = 89\%$), but numerous cycles may be needed depending on the CSR. Specimens with a higher relative density D_r had higher liquefaction resistance. The excess pore water pressure generated during the cyclic loading nearly reached the $\sigma'_{v0} = 100$ kPa when the shear strain of the specimen exceeded 3.75% single amplitude.
- PM response of the liquefied specimens can be categorized into three distinct stages. Initially, no significant increase in shear stress was observed until vertical effective stress started increasing. With a further increase in shear strain, an increase in the shear stress was observed, which was more pronounced for the higher densities. Loosely packed specimens required larger postcyclic shear strains before the onset of an increase in shear stress. Overall, substantial postcyclic shear strain is required to mobilize postcyclic monotonic shear resistance following liquefaction of the soil.
- All PRM tests presented more pronounced shear stress development than monotonic tests. This can be mainly attributed to the densification effects and associated stiffer soil skeleton formed during postcyclic reconsolidation. The results show that higher relative density D_r specimens reached higher shear stress, indicating that the degree of vertical effective stress recovery (i.e., dissipation of excess pore water pressure) is critical in determining postcyclic monotonic shear resistance.
- Postcyclic volumetric strain was primarily affected by the maximum shear strain experienced during cyclic loading: a higher maximum shear strain resulted in higher postcyclic volumetric strain. The postcyclic volumetric strain reached its ultimate values at a shear strain of 7%–15%, depending on the relative density D_r. The postcyclic volumetric strain relationship with the cyclic shear strain of this well-graded sandy gravel can be fitted with a hyperbolic model. The well-graded gravelly soils have lower ultimate postcyclic volumetric strain than clean sands. This lower postcyclic volumetric strain potential could be related to the packing characteristics of the soil and the relatively small range between its maximum and minimum void ratios.
- Comparison of virgin M, PM, and PRM tests reveals that shear stress ratio $(\tau/\sigma'_v)_{10}$ is primarily affected by the relative density D_r and vertical effective stress σ'_v, which is related to the generation and dissipation of pore water pressure. Also, high number of cycles N_c can result in a reduction of shear stiffness and strength as a secondary factor.
- Shear wave velocity V_S of well-graded gravelly soils ranged from 194 to 246 m/s at vertical effective stress $\sigma'_v = 100$ kPa, depending on relative density D_r. After liquefaction and before reconsolidation, the specimens showed an even lower V_S than the values expected only considering the reduction of σ'_v. Subsequent reconsolidation of the specimens increased V_S and reached a slightly higher V_S than before liquefaction at initial vertical effective stress σ'_{v0}, which is primarily attributed to densification effects and fabric change.

Data Availability Statement

Some or all data, models, or code that support the findings of this study are available from the corresponding author upon reasonable request.

Acknowledgments

This research was supported by the National Science Foundation (NSF) under Grant No. CMMI-1663288, a Pacific Earthquake Engineering Research (PEER) Center grant and the New Zealand QuakeCore Center. Any opinions, findings, conclusions, and recommendations expressed in this paper are those of the authors and do not necessarily reflect the views of the NSF, PEER or NZ QuakeCore. The authors would like to thank Sean Rees from the Univ. of Canterbury, NZ, for assistance with soil specimens transport to UC Berkeley.

References

Andrus, R. D., and K. H. Stokoe II. 2000. "Liquefaction resistance of soils from shear-wave velocity." *J. Geotech. Geoenviron. Eng.* 126 (11): 1015–1025. https://doi.org/10.1061/(ASCE)1090-0241(2000)126:11(1015).

ASTM. 2006. *Standard test methods for minimum index density and unit weight of soils and calculation of relative density.* ASTM D4254-00. West Conshohocken, PA: ASTM.

ASTM. 2007. *Standard test methods for consolidated undrained direct simple shear testing of cohesive soils*. ASTM D6528-07. West Conshohocken, PA: ASTM.

ASTM. 2012. *Standard test methods for laboratory compaction characteristics of soil using standard effort*. ASTM D698-12e2. West Conshohocken, PA: ASTM.

Athanasopoulos, G. A., G. C. Kechagias, D. Zekkos, A. Batilas, X. Karatzia, F. Lyrantzaki, and A. Platis. 2020. "Lateral spreading of ports in the 2014 Cephalonia, Greece, earthquakes." *Soil Dyn. Earthquake Eng.* 128 (Aug): 105874. https://doi.org/10.1016/j.soildyn.2019.105874.

Basham, M., A. Athanasopoulos-Zekkos, and D. Zekkos. 2019. "The importance of vertical displacement control during constant volume cyclic direct simple shear testing." In *Proc., 7th Int. Conf. on Earthquake Geotechnical Engineering for Protection and Development of Environment and Constructions*, 1354–1361. Boca Raton, FL: CRC Press.

Bolton Seed, H., K. Tokimatsu, L. F. Harder, and R. M. Chung. 1985. "Influence of SPT procedures in soil liquefaction resistance evaluations." *J. Geotech. Eng.* 111 (12): 1425–1445. https://doi.org/10.1061/(ASCE)0733-9410(1985)111:12(1425).

Bray, J. D., and R. B. Sancio. 2006. "Assessment of the liquefaction susceptibility of fine-grained soils." *J. Geotech. Geoenviron. Eng.* 132 (9): 1165–1177. https://doi.org/10.1061/(ASCE)1090-0241(2006)132:9(1165).

Cao, Z., T. L. Youd, and X. Yuan. 2011. "Gravelly soils that liquefied during 2008 Wenchuan, China earthquake, Ms= 8.0." *Soil Dyn. Earthquake Eng.* 31 (8): 1132–1143. https://doi.org/10.1016/j.soildyn.2011.04.001.

Cao, Z., T. L. Youd, and X. Yuan. 2013. "Chinese dynamic penetration test for liquefaction evaluation in gravelly soils." *J. Geotech. Geoenviron. Eng.* 139 (8): 1320–1333. https://doi.org/10.1061/(ASCE)GT.1943-5606.0000857.

Cappellaro, C., M. Cubrinovski, J. D. Bray, G. Chiaro, M. F. Riemer, and M. E. Stringer. 2021. "Liquefaction resistance of Christchurch sandy soils from direct simple shear tests." *Soil Dyn. Earthquake Eng.* 141 (Aug): 106489. https://doi.org/10.1016/j.soildyn.2020.106489.

Chang, W. J., C. W. Chang, and J. K. Zeng. 2014. "Liquefaction characteristics of gap-graded gravelly soils in K0 condition." *Soil Dyn. Earthquake Eng.* 56 (Jan): 74–85. https://doi.org/10.1016/j.soildyn.2013.10.005.

Cubrinovski, M., et al. 2017a. *Geotechnical reconnaissance of the 2016 Mw7. 8 Kaikoura, New Zealand Earthquake*. *Rep. GEER-053, Ver, 1*. San Francisco: GEER Association.

Cubrinovski, M., B. A. Bradley, K. J. Elwood, D. Johnston, C. Orchiston, T. Sullivan, and L. M. Wotherspoon. 2020. "Wellington's earthquake resilience: Lessons from the 2016 Kaikōura earthquake." *Earthquake Spectra* 36 (3): 1448–1484. https://doi.org/10.1177/8755293020919426.

Cubrinovski, M., J. D. Bray, C. de la Torre, M. Olsen, B. Bradley, G. Chiaro, E. Stocks, L. Wotherspoon, and T. Krall. 2018. "Liquefaction-induced damage and CPT characterization of the reclamations at CentrePort, Wellington." *Bull. Seismol. Soc. Am.* 108 (3B): 1695–1708. https://doi.org/10.1785/0120170246.

Cubrinovski, M., J. D. Bray, C. De La Torre, M. J. Olsen, B. A. Bradley, G. Chiaro, E. Stocks, and L. Wotherspoon. 2017b. "Liquefaction effects and associated damages observed at the Wellington Centreport from the 2016 Kaikoura earthquake." *Bull. N. Z. Society Earthquake Eng.* 50 (2): 152–173. https://doi.org/10.5459/bnzsee.50.2.152-173.

Cubrinovski, M., and K. Ishihara. 2002. "Maximum and minimum void ratio characteristics of sands." *Soils Found.* 42 (6): 65–78. https://doi.org/10.3208/sandf.42.6_65.

Dhakal, R., M. Cubrinovski, and J. D. Bray. 2020. "Geotechnical characterization and liquefaction evaluation of gravelly reclamations and hydraulic fills (Port of Wellington, New Zealand)." *Soils Found.* 60 (6): 1507–1531. https://doi.org/10.1016/j.sandf.2020.10.001.

Dyvik, R., T. Berre, S. Lacasse, and B. Raadim. 1987. "Comparison of truly undrained and constant volume direct simple shear tests." *Géotechnique* 37 (1): 3–10. https://doi.org/10.1680/geot.1987.37.1.3.

Enomoto, T. 2019. "Liquefaction and post-liquefaction properties of sand-silt mixtures and undisturbed silty sands." *Soils Found.* 59 (6): 2311–2323. https://doi.org/10.1016/j.sandf.2019.09.005.

Flora, A., S. Lirer, and F. Silvestri. 2012. "Undrained cyclic resistance of undisturbed gravelly soils." *Soil Dyn. Earthquake Eng.* 43 (Jun): 366–379. https://doi.org/10.1016/j.soildyn.2012.08.003.

Fragaszy, R. J., W. Su, and F. H. Siddiqi. 1990. "Effects of oversize particles on the density of clean granular soils." *Geotech. Test. J.* 13 (2): 106–114. https://doi.org/10.1520/GTJ10701J.

Hara, T., T. Kokusho, and R. Hiraoka. 2004. "Undrained strength of gravelly soils with different particle gradations." In *Proc., 13th World Conf. on Earthquake Engineering*. Vancouver, BC, Canada: WCEE Secretariat.

Harder, L. F., Jr. 1997. "Application of the Becker penetration test for evaluating the liquefaction potential of gravelly soils." In *Proc., NCEER Workshop on Evaluation of Liquefaction Resistance of Soils*, 129–148. Buffalo, NY: National Center for Earthquake Engineering Research.

Hatanaka, M., A. Uchida, and J. Ohara. 1997. "Liquefaction characteristics of a gravelly fill liquefied during the 1995 Hyogo-Ken Nanbu earthquake." *Soils Found.* 37 (3): 107–115. https://doi.org/10.3208/sandf.37.3_107.

Hubler, J. F., A. Athanasopoulos-Zekkos, and D. Zekkos. 2017. "Monotonic, cyclic, and postcyclic simple shear response of three uniform gravels in constant volume conditions." *J. Geotech. Geoenviron. Eng.* 143 (9): 04017043. https://doi.org/10.1061/(ASCE)GT.1943-5606.0001723.

Hubler, J. F., A. Athanasopoulos-Zekkos, and D. Zekkos. 2018. "Monotonic and cyclic simple shear response of gravel-sand mixtures." *Soil Dyn. Earthquake Eng.* 115 (Jun): 291–304. https://doi.org/10.1016/j.soildyn.2018.07.016.

Ishihara, K., K. Harada, W. F. Lee, C. C. Chan, and A. M. M. Safiullah. 2016. "Post-liquefaction settlement analyses based on the volume change characteristics of undisturbed and reconstituted samples." *Soils Found.* 56 (3): 533–546. https://doi.org/10.1016/j.sandf.2016.04.019.

Ishihara, K., and M. Yoshimine. 1992. "Evaluation of settlements in sand deposits following liquefaction during earthquakes." *Soils Found.* 32 (1): 173–188. https://doi.org/10.3208/sandf1972.32.173.

Jana, A., and A. W. Stuedlein. 2021. "Monotonic, cyclic, and postcyclic responses of an alluvial plastic silt deposit." *J. Geotech. Geoenviron. Eng.* 147 (3): 04020174. https://doi.org/10.1061/(ASCE)GT.1943-5606.0002462.

JGS (Japanese Geotechnical Society). 2003. *Method for plate load test on soil ground: Japanese standards for geotechnical and geoenvironmental investigation methods – Standards and explanations*. JGS 1521-2003, 162–169. Tokyo: JGS.

Karakan, E., N. Tanrinian, and A. Sezer. 2019. "Cyclic undrained behavior and post liquefaction settlement of a nonplastic silt." *Soil Dyn. Earthquake Eng.* 120 (May): 214–227. https://doi.org/10.1016/j.soildyn.2019.01.040.

Kokusho, T., T. Hara, and R. Hiraoka. 2004. "Undrained shear strength of granular soils with different particle gradations." *J. Geotech. Geoenviron. Eng.* 130 (6): 621–629. https://doi.org/10.1061/(ASCE)1090-0241(2004)130:6(621).

Kokusho, T., Y. Tanaka, T. Kawai, K. Kudo, K. Suzuki, S. Tohda, and S. Abe. 1995. "Case study of rock debris avalanche gravel liquefied during 1993 Hokkaido-Nansei-Oki earthquake." *Soils Found.* 35 (3): 83–95. https://doi.org/10.3208/sandf.35.83.

Kokusho, T., and Y. Yoshida. 1997. "SPT N-value and S-wave velocity for gravelly soils with different grain size distribution." *Soils Found.* 37 (4): 105–113. https://doi.org/10.3208/sandf.37.4_105.

Lee, K. L., and A. Albaisa. 1974. "Earthquake induced settlements in saturated sands." *J. Geotech. Eng. Div.* 100 (4): 387–406. https://doi.org/10.1061/AJGEB6.0000034.

Lin, P. S., and C. W. Chang. 2002. "Damage investigation and liquefaction potential analysis of gravelly soil." *J. Chin. Inst. Eng.* 25 (5): 543–554. https://doi.org/10.1080/02533839.2002.9670729.

Lin, P. S., C. W. Chang, and W. J. Chang. 2004. "Characterization of liquefaction resistance in gravelly soil: Large hammer penetration test and shear wave velocity approach." *Soil Dyn. Earthquake Eng.* 24 (9–10): 675–687. https://doi.org/10.1016/j.soildyn.2004.06.010.

Marcuson, W. F. 1978. "Definition of terms related to liquefaction." *J. Geotech. Eng. Div.* 104 (9): 1197–1200. https://doi.org/10.1061/AJGEB6.0000688.

Monkul, M. M., C. Gültekin, M. Gülver, Ö. Akın, and E. Eseller-Bayat. 2015. "Estimation of liquefaction potential from dry and saturated sandy soils under drained constant volume cyclic simple shear loading." *Soil Dyn. Earthquake Eng.* 75 (Jun): 27–36. https://doi.org/10.1016/j.soildyn.2015.03.019.

Nagase, H., and K. Ishihara. 1988. "Liquefaction-induced compaction and settlement of sand during earthquakes." *Soils Found.* 28 (1): 65–76. https://doi.org/10.3208/sandf1972.28.65.

Nikolaou, S., D. Zekkos, D. Asimaki, and R. Gilsanz. 2015. "Reconnaissance highlights of the 2014 sequence of earthquakes in Cephalonia, Greece." In *Proc., 6th Int. Conf. on Earthquake Geotechnical Engineering*. London: International Society for Soil Mechanics and Geotechnical Engineering.

Nikolaou, S., D. Zekkos, D. Assimaki, and R. Gilsanz. 2014. *Earthquake reconnaissance January 26th/February 2nd 2014 Cephalonia, Greece events, Version 1Rep.* Oakland, CA: Earthquake Engineering Research Institute.

Park, S. S., Z. Z. Nong, and D. E. Lee. 2020. "Effect of vertical effective and initial static shear stresses on the liquefaction resistance of sands in cyclic direct simple shear tests." *Soils Found.* 60 (6): 1588–1607. https://doi.org/10.1016/j.sandf.2020.09.007.

Peacock, W. H., and H. B. Seed. 1968. "Sand liquefaction under cyclic loading simple shear conditions." *J. Soil Mech. Found. Div.* 94 (3): 689–708. https://doi.org/10.1061/JSFEAQ.0001135.

Pillai, V. S., and R. A. Stewart. 1994. "Evaluation of liquefaction potential of foundation soils at Duncan Dam." *Can. Geotech. J.* 31 (6): 951–966. https://doi.org/10.1139/t94-110.

Porcino, D., G. Caridi, and V. N. Ghionna. 2008. "Undrained monotonic and cyclic simple shear behaviour of carbonate sand." *Géotechnique* 58 (8): 635–644. https://doi.org/10.1680/geot.2007.00036.

Robertson, P. K., and C. E. Wride. 1998. "Evaluating cyclic liquefaction potential using the cone penetration test." *Can. Geotech. J.* 35 (3): 442–459. https://doi.org/10.1139/t98-017.

Rollins, K. M., J. Roy, A. Athanasopoulos-Zekkos, D. Zekkos, S. Amoroso, Z. Cao, G. Milana, M. Vassallo, and G. Di Giulio. 2022. "A new V s-based liquefaction-triggering procedure for gravelly soils." *J. Geotech. Geoenviron. Eng.* 148 (6): 04022040. https://doi.org/10.1061/(ASCE)GT.1943-5606.0002784.

Santamarina, J. C., K. A. Klein, and M. A. Fam. 2001. *Soils and waves*. New York: Wiley.

Seed, H. B., and K. L. Lee. 1966. "Liquefaction of saturated sands during cyclic loading." *J. Soil Mech. Found. Div.* 92 (6): 105–134. https://doi.org/10.1061/JSFEAQ.0000913.

Sitharam, T. G., J. S. Vinod, and B. V. Ravishankar. 2009. "Post-liquefaction undrained monotonic behaviour of sands: Experiments and DEM simulations." *Géotechnique* 59 (9): 739–749. https://doi.org/10.1680/geot.7.00040.

Sivathayalan, S. 1994. *Static, cyclic and post liquefaction simple shear response of sands*. Vancouver, BC, Canada: Univ. of British Columbia.
Sivathayalan, S. 2000. *Fabric, initial state and stress path effects on liquefaction susceptibility of sands*. Vancouver, BC, Canada: Univ. of British Columbia.
Sivathayalan, S., and D. Ha. 2011. "Effect of static shear stress on the cyclic resistance of sands in simple shear loading." *Can. Geotech. J.* 48 (10): 1471–1484. https://doi.org/10.1139/t11-056.
Tsukamoto, Y., K. Ishihara, and S. Sawada. 2004. "Settlement of silty sand deposits following liquefaction during earthquakes." *Soils Found.* 44 (5): 135–148. https://doi.org/10.3208/sandf.44.5_135.
Vaid, Y. P., and W. L. Finn. 1979. "Static shear and liquefaction potential." *J. Geotech. Eng. Div.* 105 (10): 1233–1246. https://doi.org/10.1061/AJGEB6.0000868.
Vaid, Y. P., and S. Sivathayalan. 1996. "Static and cyclic liquefaction potential of Fraser Delta sand in simple shear and triaxial tests." *Can. Geotech. J.* 33 (2): 281–289. https://doi.org/10.1139/t96-007.
Vaid, Y. P., and J. Thomas. 1995. "Liquefaction and postliquefaction behavior of sand." *J. Geotech. Eng.* 121 (2): 163–173. https://doi.org/10.1061/(ASCE)0733-9410(1995)121:2(163).
Wang, Y., Y. Wang, L. Kong, and Z. Sun. 2020. "Post-liquefaction shearing behaviour of saturated gravelly soils: Experimental study and discrete element simulation." *J. Rock Mech. Geotech. Eng.* 12 (5): 1119–1130. https://doi.org/10.1016/j.jrmge.2020.01.007.
Wang, Y., and Y. L. Wang. 2017. "Liquefaction characteristics of gravelly soil under cyclic loading with constant strain amplitude by experimental and numerical investigations." *Soil Dyn. Earthquake Eng.* 92 (Aug): 388–396. https://doi.org/10.1016/j.soildyn.2016.10.029.
Wijewickreme, D., A. Soysa, and P. Verma. 2019. "Response of natural fine-grained soils for seismic design practice: A collection of research findings from British Columbia, Canada." *Soil Dyn. Earthquake Eng.* 124 (Jun): 280–296. https://doi.org/10.1016/j.soildyn.2018.04.053.
Xenaki, V. C., and G. A. Athanasopoulos. 2008. "Dynamic properties and liquefaction resistance of two soil materials in an earthfill dam—Laboratory test results." *Soil Dyn. Earthquake Eng.* 28 (8): 605–620. https://doi.org/10.1016/j.soildyn.2007.10.001.
Youd, T. L., and I. M. Idriss. 2001. "Liquefaction resistance of soils: Summary report from the 1996 NCEER and 1998 NCEER/NSF workshops on evaluation of liquefaction resistance of soils." *J. Geotech. Geoenviron. Eng.* 127 (4): 297–313. https://doi.org/10.1061/(ASCE)1090-0241(2001)127:4(297).
Zekkos, D., A. Athanasopoulos-Zekkos, J. Hubler, X. Fei, K. H. Zehtab, and W. A. Marr. 2018. "Development of a large-size cyclic direct simple shear device for characterization of ground materials with oversized particles." *Geotech. Test. J.* 41 (2): 20160271. https://doi.org/10.1520/GTJ20160271.